A low-dimensional signature of brain injury and behavioral performance

Stephen E. Clarke, Iliana E. Bray, and Paul Nuyujukian, for the Brain Interfacing Laboratory

Abstract

Reversible perturbation techniques have transformed modern neuroscience; however, much can be gained by studying the irreversible loss of neurons. Here, for the first time, we performed small electrolytic lesions through chronically implanted microelectrode arrays in the motor cortex of awake-behaving animals, permitting sustained recordings from the remaining neuron population as it adapted. This neuron knockout impaired a skilled reaching behavior, which recovered alongside changes in the recorded population activity. Despite termination of individual task-responsive neurons, similar low-dimensional structure re-emerged among the remaining neuron population. This low-dimensional signature of behavioral impairment was recapitulated in an artificial neural network model and supported by numerical simulations, providing causal evidence that motor control is redistributed across the population after neuronal loss.

Summary Sentence Population signatures of neuron loss are correlated with behavioral impairment in both biological and artificial spiking neural networks.

Introduction

Permanent inactivation studies or "knockouts," are instrumental in the study of complex biological systems (e.g., genetics). While the brain is no exception, influential lesion studies in primates have been mostly limited to large tissue ablations, behavioral assays, macroscopic measures of network reorganization, and niche clinical cases in humans.[1] Although transformative for neuroscience and medicine, these approaches do not capture the activity of damaged neuron populations at the resolution of action potentials (spikes) fired by individual neurons. Yet, it is this very level of spiking activity in which key features of motor planning and execution are thought to reside, supported by decades of research correlating neuron population recordings in motor cortex with animal behaviors.[2–7] Therefore, we performed repeatable electrolytic lesions directly through chronically implanted microelectrode arrays in the motor cortex of awake-behaving non-human primates. By seamlessly integrating recording and lesioning capabilities on a single device, a subset of task-relevant neurons can be knocked-out within the recorded population. Whereas temporary manipulations can silence neurons, they do not remove them from the circuit altogether; thus, lesions are a markedly different form of inactivation, which has become regarded as an essential tool in systems neuroscience.[1,8–10] This novel approach allows for long-term recordings of neuronal populations, before and after injury, and can be easily repeated without surgical procedure. A key objective is to answer long-standing calls from academics and government research agencies for modern, refined non-human primate injury models that accelerate the translation of basic neuroscience discoveries into clinical advances.[11–13]

Emerging brain implant technologies promise to revolutionize medicine by recording detailed spiking activity from thousands of cortical neurons, with the expectation of many thousands more in the coming decades.[14–17] Understanding these large-scale brain recordings will benefit immensely from dimensionality reduction approaches that simplify neuron population activity patterns, while still capturing most of the observed variance in the recorded data.[18–20] In addition to their practical value and clinical potential for neuroprosthetics and brain computer-interfaces,[21–25] these low-dimensional descriptions of recorded activity may actually capture neuron population-level computations that drive natural movement.[26,27] Insightful studies using temporary perturbations of population activity like thermal cooling,[28] optogenetics,[29–31] external task manipulation,[32–36] and intracortical microstimulation,[37] all indicate that correlations among a population of neurons play a deeper role in generating behavior and represent something greater than the sum of their individual responses (i.e., beyond the classic population vector[5,38–40]). Dominant correlations among the population are known to reorganize during perturbation experiments with brain-computer interfaces;[35,36] however, in this case, a causal relationship between brain activity and control of the interface is mathematically defined. Therefore, it is unclear whether these same principles apply to the control of natural movement and recovery from brain injury. Although compelling, reversible manipulations are difficult to sustain over the longer timescales of natural recovery needed to properly evaluate causal aspects of the neural code[9,41] and may lead to disparate results.[42,43] While brief reversible manipulations can bring about long timescale changes for learning and memory, they are not region specific perturbations; thus,[33,37] the field largely lacks the complementary evidence provided by small localized neuron knockouts (i.e., permanent inactivation, or termination). The array-based electrolytic lesion applied here allowed us to examine how the remaining recorded neurons adapted over days-to-weeks to support recovery of function, revealing low-dimensional correlation structure in the population spiking activity linked to voluntary reaching.[44] Establishing tractable models of the neuron population activity that control natural behavior is central to a systems neuroengineering approach to rehabilitation after brain injury.

Results

Electrolytic lesion evokes behavioral deficit Two adult male rhesus macaques, Monkeys U and H, were implanted with 96-electrode Utah arrays in motor cortex and trained on a conventional reaching task using their contralateral arm (Figure 1a; Methods). During daily recording sessions, an animal's hand movements were optically tracked and projected as a cursor onto a computer screen. Successful navigation of the cursor to one of eight radial targets and holding steady for a few hundred milliseconds within the target boundary resulted in a liquid reward. The animal then reset to the center target and the cycle repeated for thousands of trials. Each daily session consisted of a first set of reaching trials (session 1), followed by a mock lesion break, then re-presentation of the task for as many trials as desired (session 2). These daily mock lesion breaks were an important sham control[45] that prevented the animals from identifying lesion days.

Under stable task performance, the three days leading up to a scheduled lesion were designated as pre-lesion days -3, -2, and -1. Additional pre-lesion data was gathered the next day during the first session (day 0). The task was then paused and a lesion was performed by passing 150±20 μA of current for either 30 or 45s through two adjacent electrodes centered near task-modulated neurons (see Supplementary Figures S2-S6). After monitoring the animal's health, the task and all recordings were resumed for session 2. Subsequent recording sessions with this structure were performed daily until the animal's behavior recovered, and, in most cases, for months thereafter (Supplementary Figure S2). Note, the following analysis was restricted to session 1 only, which provided a period of highly engaged reaching behavior every 24 hours. These sessions were capped at 750 trials in order to 1) provide a consistent task timeline for lesion breaks 2) avoid any potential ambiguity introduced by sporadic task engagement, fatigue onset, or the waning interest that can arise during longer sessions. By design, lesions were small enough that monkeys still reached the targets with relative ease, compared to traditional injury models with palpable impairment and a significant number of failed trials following injury.[46–48] This enabled the analysis to be performed on large sets of successful trials every day in order to infer precise behavioral effects, which optimizes lesioning for sustained systems neuroscience research. The only exception was when Monkey H chose not to participate in the task following lesion 3 and for the second day after lesion 10; otherwise, normal behavior and healthy vitals were observed in the home environment.

Behavioral performance was characterized by five measures derived from the cursor position data for each reach trial (Figure 1b-e). Measures included: the reaction time after a target's appearance; movement duration, calculated as the time to reach that target successfully, minus the reaction time; maximum reach velocity (v_{max}); average angular error over the 100ms following v_{max}; and the proportion of trials in which the animal reached the target with the cursor but did not hold it there successfully, requiring more time for a corrective movement (dial-in time). This standard measure of accuracy in brain-computer interface studies[49,50] is almost exclusively zero milliseconds for reach trials with healthy monkeys, but post-lesion there might be significant increases (assessed via the Chi-Square frequency test). Distributions for all other behavioral measures were assessed for changes in both central tendency (median test) and dispersion (Fligner-Kileen's variance test), two complementary measures of how the data is influenced by the lesion (Figure 1c). Changes in central tendency reflect a general shift in behavioral performance and ability, while changes in dispersion reflect performance (in)consistency. Assessing both distribution characteristics for each behavioral measure and target follows recent advice to carefully decompose goal-oriented behaviors before proceeding with causal neuronal interventions[27,51,52] and is reminiscent of a typical clinical approach to scoring behavioral deficit. Although changes in the above measures and tests are not necessarily independent, they

often occur in isolation (Supplementary Figure S2c), and are intended to capture the perturbation of different control mechanisms in the recorded neuron population.

Given the natural day-to-day fluctuations in healthy behavioral performance, it is essential for us to differentiate between baseline variability and true lesion effects. To account for this variability and the effect of multiple testing over sequential days, we employed a false detection rate analysis[53,54] (Methods). For all lesions, each target, behavioral measure, and statistical test was assigned a *p*-value threshold by drawing 10^4 repeated trial samples with replacement from individual pre-lesion days and testing the one-sided alternative hypothesis that the sampled data was impaired with respect to the total pre-lesion set [-3,-2,1,0]. This process was repeated over the range of *p*-value thresholds (α): 10^{-2} to 10^{-12}. When the false detection rate across all pre-lesion days dropped below 1% for a given statistical test, behavioral measure, and target, that specific p-value threshold was selected for testing daily post-lesion significance for that specific set of conditions. As an illustration, day -3 for UL1 was notably worse than the other pre-lesion days and thus was the last to have its false detection rate drop below 1% for the median test on bottom and bottom-right target's move duration (Figure 1c, d). This approach systematically minimizes the likelihood of false positives for the large number of statistical tests performed here, while preserving statistical sensitivity to the hypothesized lesion effects at a 99% level of confidence.[53,54]

Significant changes in median and variance were observed following lesions, both individually and in unison (Figure 1e, Supplementary Figure S2). Distinct sets of targets and behavioral measures were affected each time and the effects could last for days to weeks. The summary panels for Monkeys U and H are based on significant differences detected for both statistical tests, summed across all days in the identified post-lesion periods for each behavioral measure (row sum, Σ_r☆; Figure 1d → e) but broken down by target. The results highlight that precisely controlled electrolytic lesions are repeatable, consistently causing sparse and heterogeneous effects on motor system output. Of the remaining two lesions, one had no significant impact on behavior (UL2) and another resulted in no participation (HL3). Note, for the following analysis combining the behavioral and neuronal data, targets will remain pooled and summed over all five measures as a marker of overall daily deficit (Σ_c☆; column sum).

The same analysis was repeated for the seemingly paradoxical one-sided hypothesis that lesions caused behavioral improvements.[55] While fewer in number than deficits, significant improvements relative to pre-lesion performance were observed during both the post-lesion and recovered periods (e.g., Figure 1c, bottom left target, significance unmarked; Supplementary Figure S2d,e).

Electrolytic lesions partially damage recorded neuron populations Electrolytic lesion current (μA) and duration (s) parameters were calibrated in previous ex-vivo studies with sheep brains and in-vivo studies with anesthetized pigs.[56] Sustained direct currents between 150-200μA were delivered for up to 600s through two adjacent electrodes on Utah arrays, one acting as an anode and the other as a cathode. For an electrode separation of 400μm, these parameters resulted in clean spheroidal ablations approximately 1-1.5mm in diameter, consistent with focal lesion sizes that cause measurable behavioral deficits in both the non-human primates and rodents.[48,57–62] While larger ablations are possible through increased current, duration, and use of non-adjacent array electrodes, we restricted our lesions for this study to the less intense parameter range of 150-170μA for 30-45s on adjacent electrodes (Supplementary Figure S2). Selection of these parameters significantly reduced the extent of full ablation in favor of partially damaged tissue, whose histology indicated a mix of live and dead neurons.[56]

In-vivo application of 150μA for 45s was next performed in a sedated 16-year-old rhesus macaque

(Monkey F; Figure 2a,c-f), which demonstrated the technique's safety and allowed us to move forward with the lesion studies presented in this study. The reconstructed lesion volume from Monkey F covers about 7% of the array's surface area (Figure 2a) and illustrates three qualitatively different types of affected tissue: ablated tissue, necrotic tissue, and partially damaged tissue that contains surviving neurons hypothesized to contribute to post-acute recovery[63] (Figure 2c-f). Despite the neuronal loss, quality waveforms are still detected on nearly all electrodes following each lesion, including the lesion electrodes themselves (Figure 2b) Despite localized loss of neurons, there are many active neurons in each electrodes' recording volume: in addition to isolated neurons found within a 30-70μm radius from an electrode tip, background spiking activity is captured from many nearby neurons in a broader region with a 150μm radius.[64] It is expected that most electrodes will continue to capture this background activity, whose averaged waveform may look indistinguishable despite loss of some individual neurons. S3. Given the recorded neurons captured by the array electrodes are such a small fraction of the dense local population, most lesioned neurons are likely to have been unrecorded (Figure S3).

The total estimated lesion volume of 1.77mm^3 is consistent with lower bound estimates of previous lesion volumes in nonhuman primate studies,[48,65] but instead favors a larger proportion of partially damaged tissue over total ablation (Figure 2g). Even if complete ablation and accounting for potential neuron loss at more distal sites, the total electrolytic lesion volume would terminate at most 2.5% of neurons within the typical motor maps dedicated to a rhesus macaque's dominant reaching arm.[66,67] This leaves the system with plenty of cortical reserve beneath the recording array and within the surrounding tissue, permitting multiple lesion recovery-cycles to be performed in a single animal. While the origins and mechanisms of damage differ, the observed partial neuronal loss is reminiscent of general ischemic/hypoxic damage in animal models and human stroke survivors (Figure 2h,i).[63,68–71] Since a viable neuronal population remains, we can continue to record the brain's local recovery process at a single-neuron resolution in an attempt to identify novel signatures of brain injury and behavioral deficit.

Population spiking activity as a signature of behavioral deficit As a quantification of total behavioral impairment for each post-lesion day, significant differences were summed across all behavioral measures, targets, and statistical tests ($\Sigma_c\star$; Monkey U, 72 possibilities; Monkey H, 54 possibilities, Figure 1). This daily deficit score was then compared to the recorded neuron population activity. Considering a significance score across all task conditions is similar to clinical assessments of brain injury and ensured sensitivity to perturbation of different component processes within the recorded neuron population, which may manifest differently in during behavioral recovery.[51]

Conventional measures of population activity demonstrated the lesion's effect on the broader neuron population, both within and beyond estimates of its physical boundary (Figure 2; Supplementary Figures S4-S6). Broad-scale changes in the peri-move beta-band local field potential (β-band LFP) across the array were a reliable indication of a lesion, providing a strong connection to clinical reports and contemporary non-human primate lesion models.[73,74] However, the changes in β-LFP power were quite variable across the lesions; in some cases activity increased following a lesion, other times it decreased (Figure 3a-c, Supplementary Figures S9, S10). While a strong indicator of an injury and seemingly an integral component of recovery, array-wide shifts in the β-band LFP power were a weak signature of behavioral performance, even after the removal of seven outliers (values exceeding the 95th percentile; r=0.08, p=0.37; see also Supplementary FigureS12a). This warranted a closer look at the fine-scale, 'high-dimensional' neuron population data (Supplementary Figures S5,S6), where each individual neuron is viewed as an independent encoder of explicit task conditions (e.g., target direction). Many interpretable neuron responses with strong directional tuning were observed, among many other neurons whose relationship to task conditions were less clear. Ostensibly different patterns

of single neuron tuning were observed over multiple lesion-recovery cycles in both animals, producing the same level of behavioral performance. This suggests that correlational structure of sampled neurons might better reflect the performance of the entire population that produces normal reaching behavior.

Dominant neuron population patterns (states) present during reaching were examined next due to the mounting evidence that population states and dynamics are foundational to behavior.[8,26] Clinical success with brain-computer interface devices that use these empirical state models reflect a valuable trade-off between capturing rich, individualized detail from neuron population recordings and identifying simple 'low-dimensional' control signals present in the population.[36,50,75] The ten largest eigenvalues (λ_{1-10}) of the peri-move population firing rate covariance matrix were computed as a percentage of the total explained variance for each daily recording session and the top three are plotted in Figure 3a,b and Supplementary Figure S7, S8. These values reflect the relative prominence of different activation patterns (i.e., principal components[76]) within the recorded neuron population during reaches for [-50, 400]ms about each trial's reaction time. After a lesion, the largest dimensions of the neuronal state space varied over days alongside changes in behavioral impairment. The changes in state were quantified by the fractional change of λ_k from the median value of λ_k observed during the pre-lesion days [-3,-2,-1,0], for $k = 1-10$ (Figure 3a,b). The absolute value of these changes were then summed as a measure of state perturbation (L_{10}). Analysis was restricted to the largest ten eigenvalues where changes were predominantly observed. Combining the results from each lesion cycle demonstrated that changes in L_{10} and the extent of behavioral deficit are significantly correlated and generalize across subjects (Figure 3d; $r = 0.49$, $p = 1.1\text{x}10^{-8}$). Note, seven easily identified outliers, the largest 5%, were also excluded here (see Supplementary Figure S12b). These results suggest that low-dimensional structure in neuron population activity may act as reliable signature of brain injury and behavioral deficit, particularly when recording a small sample of a much larger neuron population. Furthermore, the day-to-day variability of the L_{10} measure itself provides important information about network performance: when the network is impaired, its activity is likely far more constrained within a set of degenerate population patterns hypothesized to be associated with the desired motor output.[77,78] Like stimulus-evoked cortical responses,[79] variability in the population may be quenched after injury and reflected in variance of the L_{10} measure (Supplementary Figure S12b).

For the second lesion in Monkey U, there were visible changes in the firing rates of individual neurons but negligible changes in the neuronal state (median test, $p = 0.2$, compared to all pre-lesion days; $p = 0.06$, when compared to just the UL2 pre-lesion days). In this case, there were no significant behavioral deficits detected (Figure 1e, Supplementary Figure S2, S5, S7,S12c). These three null post-lesion days were combined with all intermittent post-lesion days where no behavioral deficit was detected and included in the recovered group. A slight but significant difference was detected between the medians of the pre-lesion and the recovered L_10 values ($p = 0.01$); however, in practice, the measure effectively returns to pre-lesion levels (Supplementary Figure S12c).

Finally, to test the generality of low-dimensional population activity as a signature of network performance, lesion simulations were performed in a recurrent and fully connected spiking neural network.[80] A population of 1000 neurons was modeled with leaky-integrate and fire dynamics and connectivity weights were set to produce population activity like that observed in motor cortex[81] using the Nengo Python package.[82] The network is trained to reproduce an input signal as an output, providing a proxy for behavioral performance that is characterized by the residual square error between the two signals. Repeated simulations varied the fraction of ablated neurons (0 through 0.75) and the same dimensional reduction analysis was performed on random, noisy samples of 96 neurons. Each simulation provided a scatter point of the residual square error and changes in L_{10}, which were then

fit with linear regression (r=0.45, p=3.8x10^{-185}). These simulations provided a distinct source of supporting evidence[83] for the relationship between state and performance, as well as insight into the observed experimental variability; identical fractions of ablated neurons could have varying levels of effect on performance. The model also predicted the presence of the observed pre-lesion outliers and produced comparable *r*-values (Supplementary Figures S11 and S12). To verify that the changes in the low-dimensional state were not simply increasing as a consequence of substantial rank reduction, but instead a meaningful redistribution of the largest eigenvalue magnitudes, neuron loss was analyzed in structured random matrices. Changes in the eigenvalue distribution shape were prominent, while the sum of the top 10 eigenvalues was far less influenced (Supplementary Figure S13).

Discussion

Population activity, lesions, and causal necessity With access to ever-larger population recordings from microelectrode arrays and imaging technologies, neuroscience has experienced a paradigm shift in which "neuronal dimensions," reflecting coordinated activity patterns of many individual neurons, act as a robust basis of information and that it's their time-varying activation that controls behavior.[15,26,84] Substantial evidence from multiple brain regions, species, and even artificial neural networks support this perspective based on the application of dimensional reduction techniques to neuron population spiking activity that is correlated with task behaviors.[3,4,15,26,85–96] However, just because there is a correlation between measures of neuron population activity and a behavior doesn't mean it's causally necessary to produce that behavior;[1,8,51,97] some elements of population activity may be unrelated or even epiphenomenal, cluttering our view of true neuronal computation.[8,26] Alternatively, some low-dimensional measures of population activity may be insufficient, missing important details of the neuronal code that challenge current model assumptions.[15,20,98]

The electrolytic lesion presented in this article permanently inactivated subsets of recorded neuron populations in motor cortex, resulting in behavioral deficits on a skilled reaching task. Since behavior could be recovered, we can conclude that the individual terminated neurons themselves *were not causally necessary* in generating behavior. After repeated lesions, even more neurons were lost, yet behavior was largely restored after adaptation by the remaining population. The heterogeneous effect of our experimental and simulated lesions on the exact neurons terminated, as well as the unique behavioral outcomes, demonstrate that the connection observed here between population state activity and reaching performance holds up to randomization.[10,27] Behavioral heterogeneity was also present despite repeated lesions in nearly the same location; this might be unusual for a highly topographic area like primary visual cortex,[99] but is not surprising given the complicated topographical organization of primary motor cortex.[100] An intriguing alternative to the controlled randomness associated with physical and electrical lesions would be highly specific neuron deletions using new tools that enable induction of programmed cell death through light-activated caspase proteins.[101,102]

Changes in behavior were found to significantly correlate with changes in the top dimensions of a standard population state analysis, whose relative magnitudes were largely restored after behavioral recovery (Supplementary Figure S12c). This provides strong evidence for our main hypothesis: altered neuronal state implies behavioral deficit. Importantly, one lesion did not significantly alter behavior providing a valuable control. Despite terminating a subset of the local neuron population, the recorded changes in state were typical of pre-lesion day set (median test, p =0.2; Supplementary FigureS7) consistent with the logical contrapositive of our main hypothesis: no behavioral deficit implies no altered neuronal state. While individual neuron tuning was altered in this behaviorally-null lesion,

these changes did not impair reaching task performance (UL2; Figure 1e, 3d, Supplementary Figures S5, S7). This finding was observed in general for intermittent days with recovered behavior following a lesion (Supplementary FigureS12c). Monitoring real-time voltage and the current that passed through the lesion device[56] during this behaviorally-null lesion confirms that motor cortex experienced conditions that should terminate thousands of neurons. In this case, despite the loss of individual task-relevant neurons, the emergent correlational properties of the network were largely unperturbed among the remaining neurons that support goal-directed reaching..[26,103] Although it could be argued that the null lesion simply resulted from an out-sourcing of motor control to distal networks, this seems unlikely given two subsequent lesions through the same array caused prolonged behavioral deficits and significant network re-organization during recovery of behavior (Figures 1, 3 and Supplementary Figures S2, S5, S7).

Further confidence in the connection between low-dimensional states and behavior was provided by an artificial spiking neural network model, whose use in neuroscience as an experimental tool has risen to prominence.[73,80,104–107] These model network simulations provided a unique opportunity to sample true causal relationships, since a direct mapping from stimulus to response is local, lying entirely within the defined network's connectivity.[81] By randomly and repeatedly deleting a specific fraction of neurons and assessing the effect on network performance, we effectively simulated termination of groups of neurons with varying degrees of importance to a network (Figure S11). The model results demonstrated the intuitive hypothesis that more terminated neurons lead to worse behavioral performance, but with many cases where smaller fractions of terminated neurons affected behavioral performance more than larger terminated fractions. While by no means an exhaustive exploration of the model, the selected parameters illustrated the same qualitative trend and variability observed *in vivo* (Supplementary Figure SS12). The agreement between biological and artificial neural networks suggests that the neuronal population state could be a useful measure of behavioral impairment that captures at least some of the causal network-level organization that controls reach behavior. The proposed here, L_{10}, is not a specific coding mechanism and its relationship to behavior is not perfect (Figure 3a,b). Despite a positive linear trend between network impairment and L_{10}, outliers were observed (Figure 3; Supplementary Figures S11, S12). Likely sources of variability in daily eigenvalues and L_{10} include: sub-sampling neuron correlations from a much larger network, complicated further by gradual neuron turnover.[89]; high network degeneracy,[77] in which many network configurations can occur over time to produce a desired outcome;[108] and occasional disengagement of motor cortex,[109] where the brain may be relying on other motor regions for voluntary reaching (e.g., supplementary motor area and the reticular formation[110–112]). More sophisticated models than the linear spectral decomposition presented here may also improve predictive performance and potentially decrease the impact of these outliers. Employing non-linear dimensionality reduction would likely better describe the low-dimensional population activity, as recently evidenced in rodent hippocampus..[96] Descriptions of task performance that account for exact differences in the continuous valued behavioral measures are anticipated to further improve the above relationship. While multi-variate probabilistic models of behavior will be explored subsequently, the approach taken here embraces a clinical-like score as an overall reflection of performance.

A novel primate lesion model There have been longstanding calls for modern injury models that largely remain unmet;[113] this prompted a recent re-iteration from the US National Institutes of Health, which emphasized the need for nonhuman primate models that accelerate translation of basic science findings into viable clinical therapies for brain injury (e.g., stroke).[12] The pursuit of the new primate lesion model presented here was grounded in the "three Rs" of ethical animal research:[114] refinement, reduction, and replacement. Unfortunately, model simulations and lower-level

mammals sit at the beginning of the translational pipeline and cannot fully *replace* nonhuman primates, whose relative anatomical, physiological, and behavioral homology to humans makes them central to launching clinical trials.[13,115] Of these non-human primates, old world rhesus macaque monkeys are the most robust lab animal, with decades of supporting research and a demonstrated impact on the translation of basic systems neuroscience into clinically impactful brain-computer interface technologies and neuroprosthetics.[23,50,116] Primate research strives to *reduce* the number of animals used, which is the rationale for only presenting histology from a single lesion on a geriatric animal, Monkey F, having first performed extensive calibrations *ex vivo* and *in vivo* with anaesthetized sheep and pigs destined for medical research.[56] By balancing both scientific and ethical considerations, this technique presents a *refined* approach to nonhuman primate lesion studies. The key innovation is the use of a microelectrode array to gather detailed neuron activity and perform precise, surgery-free lesions on alert animals. These electrolytic lesions can be repeated multiple times with no tangible effect on the animal's daily behavior outside of precision task performance. The small lesion volumes and reduced levels of ablation have the additional benefit of minimizing the confounding effects of connectional diaschisis (i.e., the alteration of distal unrecorded brain areas evoked by the local neuron loss).[10,117]

The number of neurons found under one mm^2 of flattened macaque motor cortex is 50,000 for hand/arm areas.[67] Surface depth suggests that the electrolytic lesion was contained mostly within cortical layer 2/3 and covered roughly $1mm^2$ (Figure 2). Therefore, we estimate a local population of about 267,000 neurons near the $16mm^2$ array. The lesion itself covers roughly $1mm^2$ and thus may have terminated as many as 17,000 neurons. Additional neuron loss is expected beyond the visible lesion boundaries due to decreases in membrane integrity and secondary death resulting from current spreading along low resistance pathways like axon bundles or the interstitial fluid surrounding blood vessels. This hypothesis is consistent with Figure 2b, where recorded neuron waveforms well beyond the immediate lesion zone were affected by putative neuron loss.Estimation of neuron loss using numerical simulations was illustrated with the spiking neural network model and then applied to the *in vivo* population data (Figures S13 and S14). This approach yielded estimates ranging from 14,000 to 76,000 lost neurons for the lesion parameters 30-45 seconds and 150±20μA of current. These estimates further suggest that neuron loss was experienced beyond the immediate lesion boundaries.

Estimates of neuron loss during an ischemic attack in humans suggest that approximately 35 neurons/mm^3 die every minute,[118] emphasizing the fact that "time is brain" (i.e., the sooner the treated the better). Considering the total loss estimated across the array, one minute of an electrolytic lesion in Monkey U and H likely led to the termination of a few thousand neurons. This larger rate of neuron loss suggests that lesions might emulate the damage experienced in 0.5-3 hours of untreated stroke. Despite the discrepancy between rates of loss, "time is brain" is relative in patients, where the degree of circulatory collateralization and other factors can play a mojor role.[119] Thus, it is of little concern for studying the chronic endpoint, after re-perfusion,[120] in which a brain network has lost a fraction of its neurons but remains viable. At a strictly network level, an injury from an electrolytic lesion might be a reasonable approximation of population loss after a stroke, but with much smaller affected volumes (e.g., cerebral microinfarcts[71,121]). The electrolytic lesion volumes presented in this article were intended to be small, comparable to the damage arising from distal artery-targeted photothrombotic infarcts that affect skilled behaviors in rodents[61] , as well as vascular ligature and photothrombosis in primates.[57,73] The tissue surrounding the core of the electrolytic lesion is characterized by partial neuronal loss, leaving behind viable neurons that have been identified as an important therapeutic target in chronic stroke survivors.[63,70,122] Given the density of motor cortex neurons and the inhomogeneous injury within each electrodes' recording volume (150μm, surviving neurons were picked

up by the electrodes even near the lesion cores (Figure 2a,b; S3). Overall, the technique spared a large reserve of reach-related neurons and the opportunity for repeated lesion-recovery cycles under the same array. Interestingly, despite our best efforts to create a controlled precise lesion,[56] the exact same parameters could have very different behavioral effects, comparable to stroke, where similarly sized and located infarcts can manifest differently in behavioral impairment.[112,123,124]

Consistent with past experimental and clinical evidence, β-LFP power during movement was affected by the electrolytic lesion and appears to be an integral part of recovery. However, β-LFP power was not always associated with improved behavioral performance. We observed consistent alteration in β-LFP power after each lesion but with varying sign; in some cases it increased, likely reflecting increased local inhibition (e.g., Figure 3a), whereas in some cases β-LFP power decreased (e.g., Figure 3b). This decrease is hypothesized to occur for larger lesions through a decreased excitatory drive on reciprocally connected motor regions and thalamus,[125,126] which results in decreased projections back to local interneurons in motor cortex. The interpretation of β-LFP as an inhibitory source is suggested by both animal and human electrophysiology,[127–129] as well as clinical evidence from stroke,[130] mild traumatic brain injury,[131] and Parkinson's disease.[132] Although electrolytic lesioning lacks precedent for studying the chronic effects of ischemic/anoxic and traumatic brain injury, seamlessly integrating lesions with recordings on implanted microelectrode arrays presents a unique opportunity to identify biomarkers of network reorganization that are causally related to the recovery of skilled behavior in the chronic stages of an injury.[63,70]

Two modes of circuit recovery Assessment of the literature provides two distinct but complementary perspectives on the re-organization of neuronal networks after injury. A common and well-supported view is that synaptic plasticity during behavioral rehabilitation can improve outcomes by forming new connections between neurons remaining in motor cortex and *re-mapping* the original relationships that drive behavior.[122] An emerging alternative view is that network mechanisms can *recover* relationships in population activity through rapid circuit re-configurations that favor different coordinated patterns of spiking activity that lead to the same behavioral outcome (i.e., leveraging degeneracy in the population, a phenomena evidenced on slower timescales by cortical drift[77,87,89,133–136]). These operations likely involve some forms of synaptic plasticity and gain control, but not the extensive plasticity involved in remapping new task relationships among spared neurons.

Re-learning by network reallocation Animal injury models suggest that windows of recovery allow for enhanced excitability and reallocation of motor control within the remaining network.[122] Studies analyzing behavior and motor maps in nonhuman primates provide significant evidence of reallocation after injury, provided sufficient behavioral training is pursued.[57,65,137,138] Interestingly, on the eighth day after lesion 4 in Monkey H, lesion 5 was performed despite the fact that the system had not recovered, providing an interesting case study. Although this lesion presumably contributed to the deficits measured on the 9th and 10th post-lesion days, it was then followed by a dramatic behavioral recovery (Figure S2,3b). Although counter-intuitive, this effect has been described in rodents, where a second stroke can lead to behavioral recovery by re-opening putative plasticity windows for reallocation.[55,122] Clinical research has since found evidence consistent with a period of enhanced synaptic plasticity in the human brain after stroke, in which behavioral rehabilitation training is expected to be especially effective.[139] At the extreme end of this type of recovery mechanism is a complete remapping of function to previously distinct circuits,[140] motor maps and brain regions (vicariation), observed in humans for large strokes and amputations.[141,142] However, despite its importance, remapping comes with a significant metabolic cost. Since the extensive synaptic plasticity is also reliant on concurrent behavioral training,[57,65] it is vulnerable to recovery plateaus, compensatory strategies, and sub-optimal training environments.[143]

Recovery through network reconfiguration Rodent studies have demonstrated that network compensation after damage can be implemented without the need for long-term synaptic plasticity between spared neurons attempting to take on lost function.[144] Theoretical work has provided further insight into a potential compensation mechanism, which operates on millisecond timescales through the coordinated re-balancing of network excitation and inhibition.[145] In line with these findings, optogenetic manipulation studies in rodents have demonstrated rapid re-balancing by perturbing the parvalbumin-expressing interneurons that form potent inhibitory synapses around the cell body of excitatory pyramidal neurons.[146] Suppressing these interneurons did not simply reduce inhibition onto the cortical pyramidal neurons, but instead evoked a tightly coordinated increase in both excitation and inhibition that produced nonlinear changes in tuning. The fluctuations in behavioral performance observed for different targets and measures, occurring from day-to-day, seem too fast and arbitrary to be explained entirely by purposeful remapping of function. Potentiated inputs from local and remote sources that shift the balance of excitation and inhibition may be consistent with the observed sequences of behavioral deficit and improvement observed experimentally. It could be that the observed shifts in β-LFP reflect adaptation of the excitation/inhibition ratio that help recover similar patterns of co-activation among neurons remaining in the population. When this balance is successful,[145] lesion damage may not manifest experimentally at all (e.g., UL2, Figure 1e) or be mild (e.g., UL1, UL4, and H2); conversely, when the system reaches a point where the balance of excitation and inhibition cannot be restored, the damage becomes symptomatic and sustained (recovery boundary) at which point re-mapping may become necessary. This may have been the case for the more impaired lesions U3, H4-8, and H9-10.

These two distinct modes of recovery are both important[147] and may depend on the spatial extent of the lesion and degree of neuronal loss.[123] The combined experimental and clinical evidence in the literature suggest both mechanisms may be employed for the volumes evoked by our electrolytic lesion, and that they could be targeted with neuromodulatory therapies.[147,148] Thus, the injury model presented in this article is well-suited to better understand the relationship between functional connectivity, population state models, the local field potential, and excitation/inhibition ratios, while further providing the ability to stimulate the population through the array to assess the impact of neuromodulation on recovery.[1,73,74,148,149]

Motor re-learning At a cellular and molecular level, recovery from brain injury is largely driven by the same systems that underlie learning and memory.[122,150] It has been suggested that endogenous synaptic plasticity during critical periods[55,151] may provide a new neuronal substrate, in which lost function (a motor engram), is partially re-allocated to a subset of neurons in the remaining population (a recovery engram).[46,122] Is the relationship between stroke recovery and motor learning also similar at a network level in partially damaged neuron populations? The random turnover in affected targets and behavioral measures observed here during recovery appear consistent with exploration of the state space during motor learning, a phenomena recently demonstrated in brain-computer interface studies with rhesus monkeys.[152,153] Whether a function of internal states such as motivation and arousal during learning, or directly from neuron loss and related sensorimotor error signals after injury, population activity in motor cortex is inevitably shifted in the neuronal state space in a potentially non-task specific manner.[153] In other words, shifts in state may arbitrarily affect behavioral performance for different targets and behavioral measures.[152] These population perturbations enable exploration of the state space and selection of beneficial patterns over time, which is consistent with the transient and variable target-specific deficits and improvements seen after electrolytic lesions for the different behavioral measures examined here (Figure 1, Supplementary Figure S2c-e). Provided there is sufficient cortical reserve, it may be that recovery from a motor cortex lesion is governed by the same

network principles as motor learning, adapting similarly to a perturbation, be it from internal failure after injury or a discrepancy between intended and desired outcomes during skill acquisition. This perspective casts injury recovery as motor re-learning within a broader framework that seeks to minimize differences between internal expectations and observed actions.[32,77,154–156] A better understanding of this relationship is expected to facilitate the design of flexible, high-performing brain implants.

Methods

Two adult male rhesus macaques, Monkeys U (aged 11) and H (14), were presented with a center-out, radial reaching task during simultaneous recordings from primary motor cortex using 1.5mm platinum shank Utah multielectrode arrays for Monkey U and 1.0mm platinum shank Utah multielectrode arrays for Monkey H (Blackrock Microsystems, Salt Lake City, Utah, USA). Both animals had stable multielectrode arrays for years prior to the studies described here. Monkey U was implanted with three arrays in the left medial and lateral primary motor cortex, as well as premotor cortex, and performed reaches with his preferred right arm. Monkey H was implanted with two arrays in the right primary motor cortex and premotor cortex and performed reaches with his preferred left arm. All animal procedures were reviewed and approved by Stanford University's Institutional Animal Care and Use Committee.

Behavioral Task Monkeys engaged in a reaching task during daily recording sessions scheduled approximately every 24 hours, seven days a week (Supplementary Figure S2). Daily data acquisition consisted of a first recording session, followed by a brief sham lesion period, then a second recording session. The sham lesion period was intended to prevent monkeys from learning to differentiate between general recording days versus those with a lesion procedure. During session 1, animals were highly engaged and limited to at most 750 successful trials, ensuring minimal confounds from fatigue or waning interest that may occur after thousands of reaches. On rare days where 750 trials were not completed in session 1, the first trials of session 2 were used to make up the difference. Otherwise, all analysis in this study is from successful trials of session 1. For both scientific and ethical reasons, lesions were calibrated to alter performance but leave overall mobility intact, resulting in very few failed trials. Participation in the reaching task was voluntary: when the animal actively engaged with the task, the room lights were automatically dimmed and the center target presented with a randomized, variable number and timing of re-presentations. If presented with inactivity the task would automatically time out, remove the target, and turn the lights back on. The task re-presented itself according to a variable schedule offering animals subsequent opportunities to play. If multiple re-presentation cycles elapsed without any play, the monkey was returned to his home environment and the day was marked as no participation (see Supplementary Figure S2).

To track reach kinematics, a reflective bead was comfortably secured to the third and fourth digits of the hand (proximal phalanges) and optically tracked at 60Hz in three-dimensions with an infrared imaging system (Polaris Spectra, Northern Digital Inc., Waterloo, Canada). The bead's position was projected onto a computer screen as a task cursor and aligned in a virtual work space so that when the animal extended the arm straight out, the cursor mapped to the origin (0,0). This ensured centered visual alignment without having to reach across the body. The task also enforced a maximum permitted distance from the screen along the axis orthogonal to its surface, requiring the monkeys to reach fully outward and make stereotyped movements within a defined work space of approximately $0.25m^3$.

A single task trial involved a green target (12mm diameter) appearing at the origin of the workspace (0,0) and the monkey moving its arm to place the cursor over the target, holding it within target bounds for 350 (250)ms for Monkey H (U). The task is illustrated in Figure 1a,b); next, one of eight radial targets appeared at a fixed interval of $\pi/4$ around an invisible circle with a radius of 100mm–this was done randomly within repeated cycles of the eight target set to ensure even trial counts, while also avoiding any potential confounds target location prediction. The monkeys reacted to the target's appearance and moved their arm to guide the cursor accordingly. Successful navigation of the cursor to the target and holding within its bounds earned a juice reward. The target then reset to the center and the cycle was repeated for hundreds to thousands of trials at the monkeys' discretion. Note, sessions with Monkey H omitted the bottom and bottom-left targets due to an apparent visual field deficit that presented during initial task training. Measures of task performance were derived from the cursor position data for each reach trial, which was synchronized with the neuronal data collected from the microelectrode array(s). Once behavioral performance was deemed stable, electrolytic lesions were performed through the recording array on day 0 during the break period between session 1 and session 2.

Behavioral Data Analysis Data streams from the infrared camera, rig lights, juicer system, and the task computer were collected, synchronized, and controlled at 1kHz using the Brain Interfacing Lab's open-source platform for realtime processing, LiCoRICE.[157] The five behavioral measures presented in this study were obtained from the time-varying two-dimensional cursor position data, differenced and smoothed using a Savitzky-Golay filter of order 2 and window length 100ms in order to estimate the second temporal derivative, cursor acceleration. During individual reaching trials, the derived acceleration profile was used to identify reaction time (react; ms) as the last positive acceleration event occurring after the appearance of the radial target ($t = 0$ in trial time) that preceded a large gap greater than 100ms. Move duration (move, ms) was calculated as the time from when the target was successfully acquired, minus the reaction time. The last negative acceleration mid-reach, just prior to initial target acquisition, is when velocity reached its maximum value, v_{max}mm ms^{-1}). This point reflected the monkey's committed reach toward the desired target. Thus, for the 100ms following this deceleration time point, a cursor heading angle was calculated relative to the direct line from the cursor position to the target. These 100 angular error values were then averaged to produce the measure θ_{error} (radians). The final measure considered was dial-in time (ms), which is the time elapsed between when the cursor first reaches the target, and when the cursor last reaches the target before a successful hold and reward. This measure of performance[50] assesses the ability to move the cursor to a target and keep it steady without slipping out and having to make corrective movements. The measures considered here are a good representation of task behavior but are not exhaustive and do not directly account for features such as movement of the arm in three-dimensions or muscle force production.

Distribution-free tests of the median (median test) and variance (Fligner-Kileen's test) were repeated for each behavioral measure on each post-lesion day with the null hypothesis that there is no difference from pre-lesion days [-3,-2,-1,0]. Dial-in time was the exception since for healthy animals its value is zero milliseconds for nearly all trials. Given the overall low incidence of non-zero dial-in times, directly comparing its duration in milliseconds, before and after a lesion, is statistically under-powered. However, comparing a simple binary measure, zero or non-zero, is suitable. The correct test in this instance is a Chi-square frequency test on the proportion of non-zero events among all trials on a given day, relative to the pre-lesion data set.

Natural fluctuations in healthy behavioral performance occur day-to-day, therefore, it is essential for us to differentiate between baseline variability and true lesion effects when performing the aforementioned

statistical tests. To account for this inherent variability, we employed a false detection rate analysis, which has the additional benefit of mitigating the effects of multiple testing over sequential days without sacrificing statistical power.[53,54] A benefit of this analysis is that appropriate *p*-value thresholds (α) can be determined by the day-to-day variability for each animal, lesion, target, behavioral measure, and statistical test; this produced a fair comparison of significance across all of the different conditions at a 99% confidence interval (Figure 1, Supplementary Figure S2). First, p-value thresholds were swept from largest to smallest over the range 10^{-2} to 10^{-12}. For each individual baseline day, the successful session 1 trials were selected and tested against the total set of corresponding baseline days' session 1 trials under the one-sided alternative hypothesis that behavioral performance was worse. This was repeated 10,000 times on trials re-sampled with replacement to get a false detection rate for each monkey, lesion, behavioral measure, target, and statistical test. When the falsely detected significance for a given set of conditions dropped below 1%, that specific *p*-value threshold was selected for testing the corresponding daily post-lesion data sets. The *p*-value thresholds uncovered by this analysis ranged from 10^{-8} to 10^{-2} for both animals, highlighting the heterogeneity present in trained, stereotyped reaches and the need for careful analysis from day-to-day.

Statistical tests were performed for all behavioral measures and targets with the specific p-value thresholds determined from the false detection rate analysis. This enabled all of the distinct measures to be scored independently as a simple binary effect (significant deficit detected, 1; no deficit, 0). Two different summaries of behavioral deficit were considered in this article. First, as a measure of total impact, deficits were summed across post-lesion days and statistical tests for each monkey, lesion, behavioral measure, and target as a visual summary of the sparse effects for the 14 total lesions performed (Figure 1e, Supplementary FigureS2a). The main text summary figure is further broken down by statistical test in Supplementary FigureS2c. Second, as a quantification of total daily injury, significant deficits were summed across all targets, measures, and statistical tests on a given day ($\sum_c \star$, Figure 1,3). Recovery was loosely defined as sporadic post-lesion days that had no behavioral deficit ($\sum_c \star = 0$) detected or a contiguous period of three days after the lesion that had no (or practically no) daily counts of behavioral significance relative to the pre-lesion data set. This process uncovered that there had not been complete behavioral recovery between some of the lesions in Monkey H and thus the analysis presented in this article re-groups the original fourteen lesions into the following: H1, H2, H3, H4-8, H9-10 and UL1, UL2, UL3, UL4.

Following this same approach, the false detection rate analysis was then repeated for the other one-sided hypothesis that behavioral performance was improved by the lesion (Supplementary Figure S2d,e).

Neuronal Data Analysis In parallel with the behavioral data streams, neuronal data was sampled at 30kHz from primary motor cortex using 96-electrode Utah arrays (Blackrock Microsystems, Salt Lake City, Utah, USA). A Blackrock CerePlex E headstage was connected to the array's external CerePort to transmit a digitized signal to a Blackrock Digital Hub, which relays the signal over fiber optic cable to a Blackrock Neural Signal Processor (firmware version 6.05.02.00), which transmits neural data over Ethernet as UDP packets. The recorded signals were then saved down to a local computer and analysed offline.

Recorded 30kHz signals were high-pass filtered using a fourth order, zero phase Butterworth filter with a 250Hz cutoff frequency. The root mean square voltage was computed for each electrodes' high-pass filtered data from different time points during the session, and, if any of these RMS blocks displayed values greater than 40-50μV, they were discarded as noisy or corrupted channels. Action potentials were identified by thresholding the filtered membrane potential at $-4\times$ the root mean square voltage

for Monkey H and -3× for Monkey U, measured over the first minute of each day's recording session. Binary rasters of spike times were determined from the identified threshold crossings. Data snippets for comparing action potential waveforms pre- and post-lesion were generated by taking the 16 sampled data points (0.53ms) before each identified threshold crossing, and the 32 sampled points (1.07ms) afterward (Figure 2b). Waveforms whose peak-to-trough amplitude exceeded 300μV are atypical of extracellular recordings from cortical neurons and were excluded.[158] Waveform width was calculated as the difference between the two prominent peaks in the temporal derivative of the extracellular potential. Waveforms whose widths were longer than 1ms were also excluded as unphysiological for fast- and regular-spiking cortical neurons.[159] The remaining waveforms were then averaged for each electrode, and event rates were determined as the number of action potentials (spikes) on a given electrode divided by the session duration. Next, each channel's data snippets were pooled and principal component analysis was performed to identify any remaining potential artifacts present in the recordings, which were subsequently removed as a spike from that channel's 30kHz raster. All binary spike rasters were then down-sampled to a 1kHz raster and aligned to the behavioral data using a serial timestamp issued every 1ms by LiCoRICE and the 30kHz timestamp issued from the Neural Signal Processor. This approach corrects for clock drift arising from data streams with independent clocks.

The neuron population activity analysed in this article was for the peri-move component of the reach (illustrated in Figure 1b). For each successful trial and each electrode, we identified the reaction time from the behavioral data and counted the spikes in the time interval 50ms before this value and 400ms after. The median change in spike counts, taken across all 450ms blocks were sorted by target direction to illustrate many classically tuned neurons,[5] as well as those that deviate (Supplementary Figures S5, S6).

For each electrode, the 450ms blocks of reach activity for all target directions were then further sub-divided into eighteen 25ms bins, in which spikes were counted to estimate a time-dependent firing rate for each trial. These time-dependent firing rates were then concatenated to form a large 96xT matrix. After subtracting the per electrode mean and scaling to unit variance, the spike rate co-variance matrix was computed, and its three largest eigenvalues (λ_{1-3}) were plotted as their percentage of the total explained variance in the data (Figure 3, Supplementary Figures S7, S8). Each set of eigenvalues represents spiking data from hundreds of successful trials, and sampling with replacement was performed 100 times on each daily trial set to ensure robust results; the median values are presented without variance since it was negligible and less visually appealing. The magnitude of these eigenvalues correspond to the magnitude of the top neuronal dimensions identified by principal component analysis.[160] For the daily L_{10} measure presented in Figure3, median values for λ_{1-10} were calculated for the pre-lesion days [-3,-2,-1,0]. On a given day, the absolute value of the fractional change from pre-lesion levels was determined for each λ_k and then summed.

The local field potential was also determined for each electrode during the same peri-move period by band-pass filtering the raw 30kHz data between 1-250Hz using a second order, zero-phase Butterworth filter. This article analyzed power in a broad β-band range of frequencies between 12 to 38 Hz, creeping a bit into the low γ range. A daily measure of activation is presented as the median β-power across all electrodes, calculated as a percent change from the median pre-lesion value ($\Delta\beta$; Figure 3). All behavioral and neuronal data analysis was performed using Python and Bash, and some computing was implemented on Sherlock, a supercomputing cluster operated by the Stanford Research Computing Center.

Network model simulations A recurrent, fully connected spiking neural network model composed

of 1,000 leaky-integrate and fire neurons was constructed by finding synaptic weights that produce integrator dynamics, like those displayed in motor cortex. This was achieved using the Neural Engineering Framework and the integrator model was implemented in the open source software package, Nengo.[81,82] As a simple and unassuming demonstration, the network's input/output dimensionality was set to two and then it was presented a one-dimensional piece-wise linear input signal, which was reproduced as output when co-activated by a control signal input. The difference between the exact input and replicated output was calculated as a residual square error and serves as a proxy for behavioral performance that is regressed against L_{10} (see Supplementary FigureS11,S12). The fraction of ablated neurons was swept from 0.0 to 0.9 by increments of 0.01, each with 25 repeated simulations that are plotted as scatter points in Supplementary Figure S11. Importantly, the exact same input signal was used for each simulation so that the observed variability is principally driven by the different network instantiations and removal of randomly selected neurons within the network. Analysis of the artificial spiking activity was done exactly as it was for the *in vivo* data, sampling 96 random neurons from the larger network to obtain sample estimates.

Electrolytic Lesions and Histology 150µA direct current was passed through two adjacent electrodes of a Utah array implanted in the dorsal premotor cortex of a sedated, male rhesus macaque for 45 seconds in an acute procedure (Monkey F; 16 years of age with unrelated health issues). Refrigeration of the animal began approximately 45 minutes postmortem. Brain tissue was extracted and fixed 16 hours later, and slices were taken in 20µm increments, then stained with Hematoxylin and Eosin (H&E). Next, slices were imaged using a SW380T compound microscope (Swift Optical Instruments, Schertz, TX) and captured using the SC500-CK 5 Megapixel digital camera (Swift Optical Instruments, Schertz TX). This set of histological images were stacked in ImageJ v1.53c (Research Services Branch, NIMH & NINDS, National Institutes of Health) and aligned based on consistent histological features using the rigid body transformation algorithm from the StackReg 2.0.0 plugin (Biomedical Imaging Group, EPFL).[161] Zones of focal ablation, coagulation necrosis, and partially damaged parenchymal tissue were identified from the surrounding healthy tissue based on color, as well as neurons' dendritic morphology and somatic vacuolation; outlines of these three zones were manually traced out over the image as Bézier curve paths in the open-source vector graphics program Inkscape (v0.92.4). The set of 2D points describing these curve paths were then exported as vector graphic files for each slide and converted to numerical Python arrays using the svgtools package (PyPi version 0.0.2). The 3D point clouds formed by the combined sets of 2D cross-sections were then fit with a convex hull using Delaunay triangulation, and transformed into a concave hull using the alpha shapes algorithm, where the simplicial complexes are formed by a set of edges and triangles that are restricted to lie within a specified radius around a given vertex. The radius parameter was set to 0.09 for this particular application as it visually represented the data best. The union of these complexes over each set form the three surface volumes shown in Figure 2a, whose combined geometry resembles the field formed by an electric dipole. The total area for each reconstructed lesion zone was determined by applying the shoelace method for arbitrary polygons to calculate the total area of each cross section, next subtracting away the area of any enclosed zones, and then multiplying each of those values by the 20µm spacing of the slices to obtain a volume in mm. Note, these estimates rely on visual demarcations in the histology and may not capture the full extent of neuronal loss in the peri-lesion tissue. Nevertheless, it is a useful approximation of lesion-evoked damage and a demonstration of the technique's ability to cause precise local neuronal loss. Although neurons found elsewhere under the array are far less likely to be damaged, some neuronal damage will almost inevitably occur at distances further from the lesion core than is detected visually. The electrical current is expected to travel along paths of least resistance near axon bundles and blood vessels, reaching out further into the tissue, albeit with diminished effect.

Animal care In the design and application of the electrolytic lesion technique described in this article, we sought solutions that adhere to the "three Rs" of animal research.[114] While non-human primates are irreplaceable in this study Supplementary Figure S1, the technique presented here significantly refines traditional lesion approaches and reduces the number of animals needed due to its repeatability, novel scientific perspective, and negligible effect on animal well-being. The work presented here necessitated careful post-lesion observation and high standards in care, which was coordinated between the Brain Interfacing Lab, veterinarians in the Department of Comparative Medicine, and animal care staff at Stanford University.

Although lesion parameters used in this study were intended to be minimal and did not yield deficits outside the precision reaching task, home environment monitoring was performed for a minimum of 6 hours after a lesion. In addition to in-person monitoring, this was facilitated using a ceiling-mounted, day/night, network camera (DNZ30TL2R, Teledyne FLIR, Thousand Oaks, CA) for remote and overnight observation. This observation took place regardless of whether any deficit was observed experimentally in case of delayed or unanticipated secondary effects of the lesion. Monkeys were evaluated again 6 hours after lesioning for further inspection and diagnostic tests. Tests included measures of body temperature via tympanic thermometer, as well as lactate and several blood gas measures taken via ear capillary blood sample (CG4+ cartridge, iStat, Abbott Labs, Chicago, Illinois, USA) Physical examination included limb strength assessment, pupil reflexes, as well as skin color and turgor. Following return to their home environment, monkeys were monitored until midnight (5 hours into night cycle) and starting as early as 4 am (3 hours before the next day cycle), in order to assess sleep quality and observe any potential unnatural postures or issues with balance (e.g., crouching or laying down on their side unnaturally). Mild restlessness during sleep was observed on some acute post-lesion nights with Monkey H (days 0-2). We did not witness any concerning signs or behavior for either animal over the course of 14 lesions and their respective recoveries.

Author Contributions

Conceptualization - PN, SEC. Data curation, SEC, IEB, PN. Formal analysis - SEC. Funding acquisition, PN. Investigation – SEC, IEB, PN. Methodology – SEC, PN, IEB. Project administration – SEC, IEB, PN. Resources – PN. Software – PN, SEC, IEB. Supervision – PN. Validation – PN, SEC, IEB. Visualization – SEC, IEB, PN. Writing, original draft – SEC. Writing, review and editing – SEC, PN, IEB.

Funding

SEC was funded by a Stanford School of Medicine Dean's Postdoctoral Fellowship, Stanford's Human Artificial Intelligence Seed Grant, and internal start-up funds awarded to PN. IEB was funded by a National Science Foundation Graduate Scholarship, a pre-doctoral fellowship from the American Heart Association, and a Stanford University Gerald J. Lieberman Fellowship. Funding for this project was mainly provided to PN by the Wu Tsai Neuroscience Institute, and supplemented from R01s NS130789 and NS123517 awarded to PN.

Competing Interests

The authors declare no competing interest.

Data and Code Availability

Data and code used in this study are available from the corresponding author upon reasonable request.

Inclusion and Ethics

The authors declare no inclusion or ethics concerns for this study. The experiments were accomplished entirely using the resources and physical space allocated to the Brain Interfacing Lab, Stanford University.

Acknowledgements

We thank Mackenzie J. Risch, Sam W. Baker and Kristina Lebedev for animal care, Jose Vilches-Moure and Kerri-Ann Casey for assistance with histology, and Kimberly Chin and Margaret Truong for administrative support. We thank Dan O'Shea, Lea Duncker, Laura Driscoll, and David Sussillo for manuscript feedback. In addition to the authors, the members of the Brain Interfacing Lab include Michelle S. Wechsler, Michael P. Silvernagel, Alissa S. Ling, and Elizabeth Jun. M. S. Wechsler was responsible for animal care, surgical support, and guiding behavioral training. M.P. Silvernagel and A.S. Ling provided additional animal care.

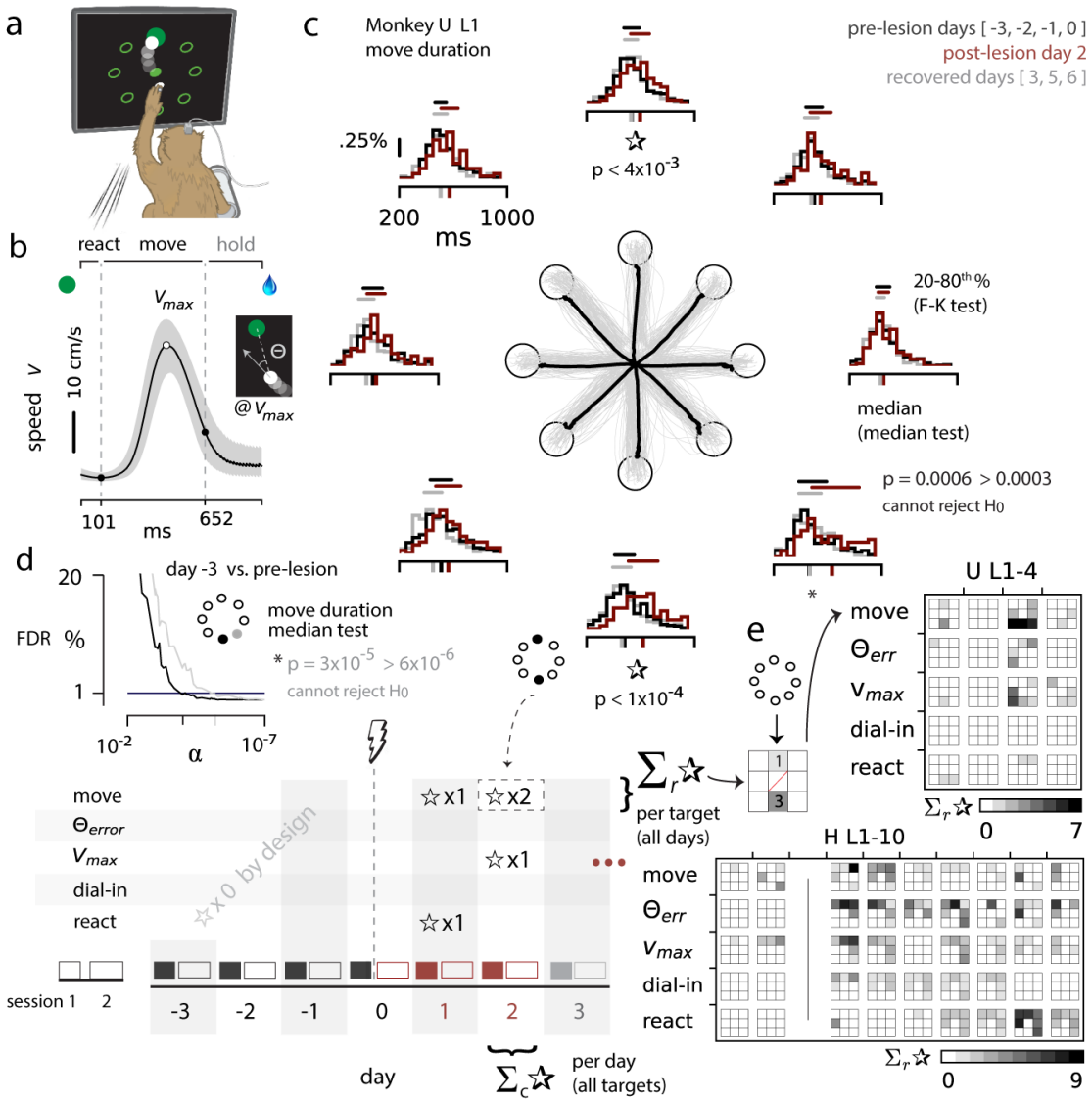

Figure 1: **Electrolytic lesions affect precise behavioral performance** a) Rhesus monkeys were implanted with 96-electrode Utah arrays in motor cortex. During daily recording sessions, stereotyped reaching moved a computer cursor to one of eight randomly presented targets, where it was held for a juice reward. b) Multiple reach features were derived from the cursor position: reaction time, move duration, reach speed (median, quartiles shown), off-target angular error, and time needed to correct if failing to hold the target (dial-in). c) Small lesions were made by passing weak electrical current through two electrodes on day 0. Histograms for the move duration feature (Monkey U Lesion 1, UL1). The median and Fligner-Kileen's tests were performed for each target to assess daily changes in median and variance, respectively (bottom, median; top, $20-80\%$ range). Unique p-value thresholds were chosen for each set of task conditions, accounting for daily sample variability and the 72(U)/54(H) statistical tests. d) *Top*: Selection of p-value thresholds for each monkey, lesion, target, behavioral measure, and statistical test, relied on a false detection rate (FDR) analysis. A range of p-value thresholds (α) were swept for all task conditions and 10^4 repeated re-samples of a given pre-lesion day's trials were tested against the entire set [-3,-2,-1,0]. When the FDR dropped below 1% for all four pre-lesion days, that α was used to test corresponding daily post-lesion significance. The bottom-right target appears affected, but its variability on pre-lesion day -3 prevented rejection of the null-hypothesis. *Bottom*: Acute deficits, UL1. The total daily deficit, Σ_c☆, is tracked as the column sum of detected deficits for all targets, behavioral measures, and statistical tests. e) To visualize each lesion's unique behavioral impact, significance was summed across days for both statistical tests, but remains broken down by reach feature and target (Σ_r☆, rows). UL2, no deficit; HL3, no participation.

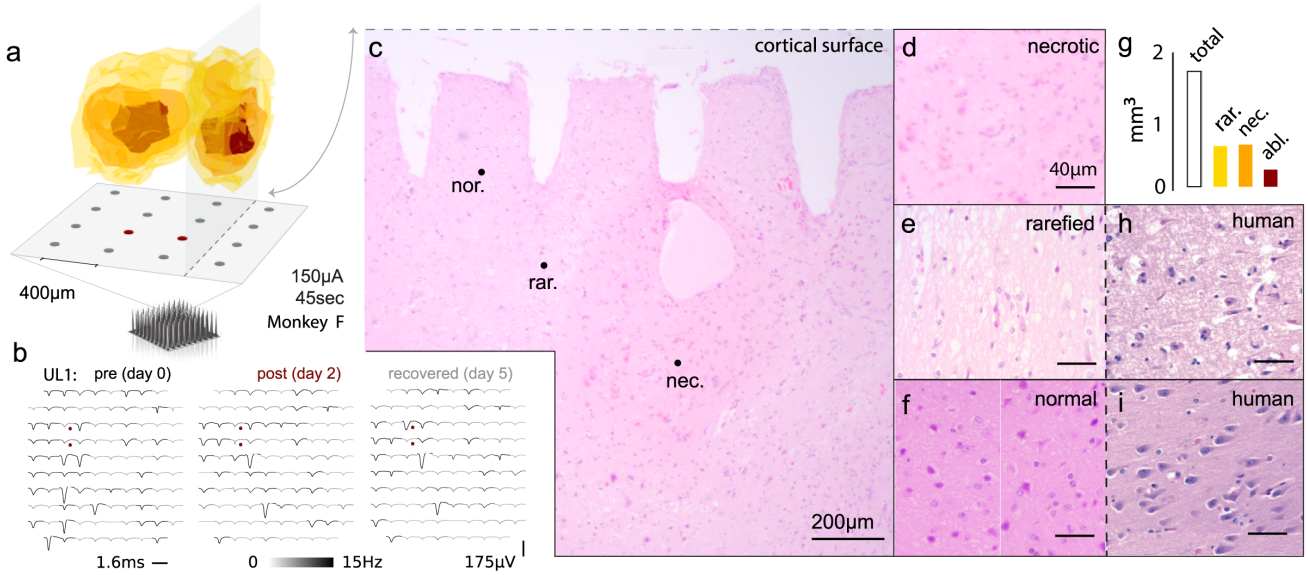

Figure 2: **Electrolytic lesions evoke neuron loss while sparing the recorded population** a) 150µA of direct current was applied *in vivo* through two adjacent array electrodes for 45 seconds (Monkey F). The approximate lesion volume was reconstructed from three visually distinct zones that were identified from cross-sectional H&E stained slices taken at 20µm increments across the 4x4mm^2 array. The focal ablation at the lesion core (red) is surrounded by a region of heat-induced coagulation necrosis (orange), and a broader region of damaged tissue characterized by rarefaction and partial neuronal loss (yellow). The extent of the visibly identified lesion is contained within approximately 7% of the array's total recording area (lesion electrodes, red dots). b) Action potential waveforms recorded from Monkey U, before and after the first lesion, illustrate the recording continuity from the implanted array. c) An example cross-sectional H&E stained slice used to reconstruct the lesion volume in panel a) (see also Supplementary FigureS3c). Note the three qualitatively distinct lesion zones; the ablated core, necrotic tissue (panel d), and partially damaged tissue (e), relative to normal looking tissue near the array's electrodes (f). The vertical indentations below the cortical surface are from the penetration of the array's electrodes, spaced 400μm apart. d) Heat coagulation creates necrotic zones, generating further neuron loss. e) Partially damaged parenchyma found proximal to the lesion core displayed light discoloration. Terminated neurons with shrunken cell bodies (somatic vacuolation) and retracted dendrites were observed. f) Histologically normal tissue from Monkey F found under the array, both near (left; shown in panel c) and far (right; not shown) from the edge of the lesion. g) The total estimated lesion volume in Monkey F was 1.77mm^3, 0.62mm^3 of which appears partially salvageable and could have contributed to recovery. h) Tissue of a 51-year old human male after a middle cerebral artery stroke (embolic infarct; reprinted with permission pending from Greenfield's Neuropathology[72]). i) Histologically normal human tissue located a few hundred micrometers away from the damaged tissue.

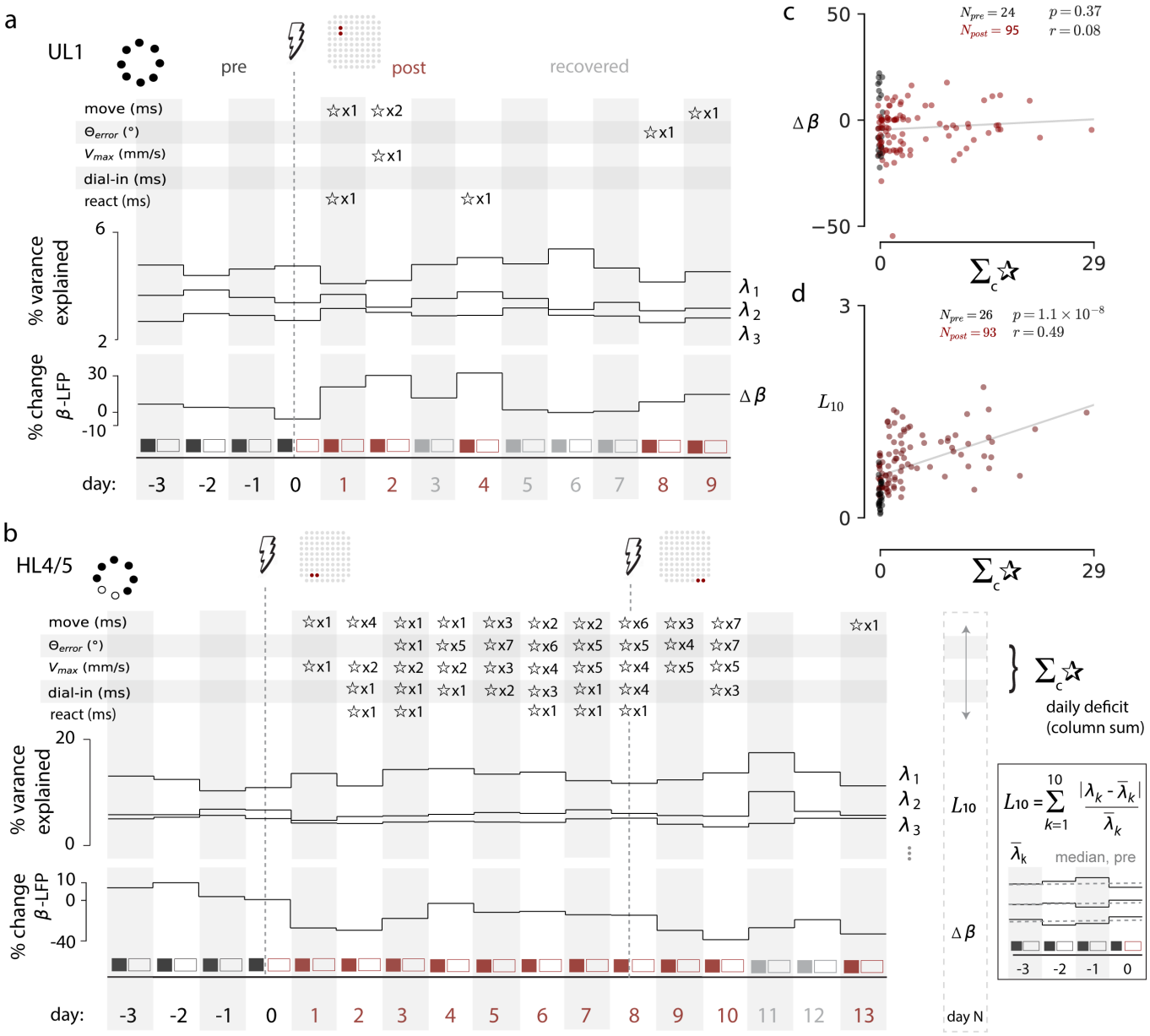

Figure 3: **Correlated population activity reflects behavioral performance** a, b) Alongside changes in behavior, lesions consistently altered population activity in Monkeys U and H. This was reflected by the eigenvalues of the peri-move spike count covariance matrix, plotted as percent contributions to the total explained variance in the recorded population data ($\lambda_{1,2,3}$ shown for UL1 and HL4/5). The median power of the peri-move β-band local field potential (LFP), measured across all 96 electrodes, is plotted below as a % change from pre-lesion median values. Behavioral deficits were summed over all targets, measures and statistical tests each day to quantify a total daily deficit ($\sum_c \star$). This significance score was compared with daily changes in β-LFP ($\Delta\beta$) and L_{10}, a measure that tracks the perturbation to the top ten eigenvalues, λ_{1-10}, relative to their pre-lesion levels. c, d) Scatter plots of ($\sum_c \star$, $\Delta\beta$) and ($\sum_c \star$, L_{10}) from all applicable lesions (Monkeys U and H). Days from the pre-lesion groups appear as black dots, whereas post-lesion days are shown in red (including recovered days, $\sum_c \star = 0$). Despite being clearly altered by the lesions, linear regression suggests β-LFP was a weak measure of behavioral performance. Alternatively, tracking changes in the low-dimensional spiking activity of neuron populations is a useful measure of behavioral deficit. Seven data points are excluded, corresponding to days where large deviations in the daily sampled eigenvalues were unusual (e.g., HL9 pre-lesion day 0, Supplementary Figure S8. This variability is consistent with the model, suggesting outliers arise as the networks are less constrained and can rely on a variety of solutions (Supplementary Figures S11 and S12).

References

[1] Vaidya, Avinash R. et al. "Lesion Studies in Contemporary Neuroscience". In: *Trends in Cognitive Sciences* 23.8 (Aug. 2019), pp. 653–671.

[2] Panzeri, Stefano et al. "The structures and functions of correlations in neural population codes". In: *Nature Reviews Neuroscience* 23.9 (Sept. 2022), pp. 551–567.

[3] Churchland, Mark M. et al. "Neural population dynamics during reaching". In: *Nature* 487.7405 (July 2012), pp. 51–56.

[4] Inagaki, Hidehiko K. et al. "Low-Dimensional and Monotonic Preparatory Activity in Mouse Anterior Lateral Motor Cortex". In: *The Journal of Neuroscience* 38.17 (Apr. 2018).

[5] Georgopoulos, A., Schwartz, A., and Kettner, R. "Neuronal population coding of movement direction". In: *Science* 233.4771 (Sept. 1986), pp. 1416–1419.

[6] Merchant, H., Naselaris, T., and Georgopoulos, A. P. "Dynamic Sculpting of Directional Tuning in the Primate Motor Cortex during Three-Dimensional Reaching". In: *Journal of Neuroscience* 28.37 (Sept. 2008), pp. 9164–9172.

[7] Tanji, J. and Evarts, E. V. "Anticipatory activity of motor cortex neurons in relation to direction of an intended movement". In: *Journal of Neurophysiology* 39.5 (Sept. 1976), pp. 1062–1068.

[8] Shenoy, Krishna V. and Kao, Jonathan C. "Measurement, manipulation and modeling of brain-wide neural population dynamics". In: *Nature Communications* 12.1 (Dec. 2021).

[9] Slonina, Zuzanna A., Poole, Katarina C., and Bizley, Jennifer K. "What can we learn from inactivation studies? Lessons from auditory cortex". In: *Trends in Neurosciences* 45.1 (Jan. 2022), pp. 64–77.

[10] Barack, David L. et al. "A call for more clarity around causality in neuroscience". In: *Trends in Neurosciences* (July 2022).

[11] Stroke Therapy Academic Industry Roundtable (STAIR). "Recommendations for Standards Regarding Preclinical Neuroprotective and Restorative Drug Development". In: *Stroke* 30.12 (Dec. 1999), pp. 2752–2758.

[12] Koroshetz, Walter. "Bridging the Translational Gap in Stroke Recovery & Rehabilitation Research". In: *Welcome Address. NIH NINDS. Rockville, MD* (2018).

[13] Higo, Noriyuki. "Non-human Primate Models to Explore the Adaptive Mechanisms After Stroke". In: *Frontiers in Systems Neuroscience* 15 (Nov. 2021).

[14] Elon Musk, Neuralink. "An integrated brain-machine interface platform with thousands of channels". In: *bioRxiv* (2019).

[15] Urai, Anne E. et al. "Large-scale neural recordings call for new insights to link brain and behavior". In: *Nature Neuroscience* 25.1 (Jan. 2022), pp. 11–19.

[16] Kleinfeld, David et al. "Can One Concurrently Record Electrical Spikes from Every Neuron in a Mammalian Brain?" In: *Neuron* 103.6 (Sept. 2019), pp. 1005–1015.

[17] Sahasrabuddhe, Kunal et al. "The Argo: A high channel count recording system for neural recording in vivo". In: *Journal of Neural Engineering* (Dec. 2020).

[18] Whiteway, M. and Butts, D. "The quest for interpretable models of neural population activity". In: *Current Opinion in Neurobiology* 58 (2019).

[19] Cunningham, John P and Yu, Byron M. "Dimensionality reduction for large-scale neural recordings". In: *Nature Neuroscience* 17.11 (Nov. 2014), pp. 1500–1509.

[20] Hurwitz, Cole et al. "Building population models for large-scale neural recordings: Opportunities and pitfalls". In: *Current Opinion in Neurobiology* 70 (Oct. 2021).

[21] Willett, Francis R. et al. "Hand Knob Area of Premotor Cortex Represents the Whole Body in a Compositional Way". In: *Cell* 181.2 (2020), pp. 396–409.

[22] Gilja, Vikash et al. "Clinical translation of a high-performance neural prosthesis". In: *Nature Medicine* 21.10 (Oct. 2015), pp. 1142–1145.

[23] Pandarinath, Chethan et al. "High performance communication by people with paralysis using an intracortical brain-computer interface". In: *eLife* 6 (Feb. 2017).

[24] Pandarinath, Chethan et al. "Neural population dynamics in human motor cortex during movements in people with ALS". In: *eLife* 4 (June 2015).

[25] Sani, Omid G et al. "Mood variations decoded from multi-site intracranial human brain activity". In: *Nature Biotechnology* 36.10 (Nov. 2018), pp. 954–961.

[26] Vyas, Saurabh et al. "Computation Through Neural Population Dynamics". In: *Annual Review of Neuroscience* 43.1 (July 2020), pp. 249–275.

[27] Jazayeri, Mehrdad and Afraz, Arash. "Navigating the Neural Space in Search of the Neural Code". In: *Neuron* 93.5 (Mar. 2017), pp. 1003–1014.

[28] Banerjee, Arkarup, Egger, Robert, and Long, Michael A. "Using focal cooling to link neural dynamics and behavior". In: *Neuron* 109.16 (Aug. 2021).

[29] Finkelstein, Arseny et al. "Attractor dynamics gate cortical information flow during decision-making". In: *Nature Neuroscience* 24.6 (June 2021), pp. 843–850.

[30] Sauerbrei, Britton A. et al. "Cortical pattern generation during dexterous movement is input-driven". In: *Nature* 577.7790 (Jan. 2020).

[31] Inagaki, Hidehiko K. et al. "Discrete attractor dynamics underlies persistent activity in the frontal cortex". In: *Nature* 566.7743 (Feb. 2019).

[32] Sun, Xulu et al. "Cortical preparatory activity indexes learned motor memories". In: *Nature* (Jan. 2022).

[33] Vyas, Saurabh et al. "Neural Population Dynamics Underlying Motor Learning Transfer". In: *Neuron* 97.5 (Mar. 2018), pp. 1177–1186.

[34] Stavisky, Sergey D. et al. "Motor Cortical Visuomotor Feedback Activity Is Initially Isolated from Downstream Targets in Output-Null Neural State Space Dimensions". In: *Neuron* 95.1 (July 2017).

[35] Golub, Matthew D. et al. "Learning by neural reassociation". In: *Nature Neuroscience* 21.4 (Apr. 2018), pp. 607–616.

[36] Sadtler, Patrick T. et al. "Neural constraints on learning". In: *Nature* 512.7515 (Aug. 2014), pp. 423–426.

[37] Vyas, Saurabh et al. "Causal Role of Motor Preparation during Error-Driven Learning". In: *Neuron* 106.2 (Apr. 2020), pp. 329–339.

[38] Seung, H S and Sompolinsky, H. "Simple models for reading neuronal population codes." In: *Proceedings of the National Academy of Sciences* 90.22 (Nov. 1993), pp. 10749–10753.

[39] Schwartz, Andrew B. "Movement: How the Brain Communicates with the World". In: *Cell* 164.6 (Mar. 2016), pp. 1122–1135.

[40] Schwartz, Andrew B. "Useful signals from motor cortex". In: *The Journal of Physiology* 579.3 (Mar. 2007), pp. 581–601.

[41] Yoshihara, Motojiro and Yoshihara, Motoyuki. "'Necessary and sufficient' in biology is not necessarily necessary – confusions and erroneous conclusions resulting from misapplied logic in the field of biology, especially neuroscience". In: *Journal of Neurogenetics* 32.2 (Apr. 2018), pp. 53–64.

[42] Bell, Andrew H. and Bultitude, Janet H. "Methods matter: A primer on permanent and reversible interference techniques in animals for investigators of human neuropsychology". In: *Neuropsychologia* 115 (July 2018).

[43] Jeurissen, Danique et al. "Deficits in decision-making induced by parietal cortex inactivation are compensated at two timescales". In: *Neuron* 110.12 (June 2022), pp. 1924–1931.

[44] Marinescu, Ioana E., Lawlor, Patrick N., and Kording, Konrad P. "Quasi-experimental causality in neuroscience and behavioural research". In: *Nature Human Behaviour* 2.12 (Dec. 2018).

[45] Landeros-Weisenberger, Angeli et al. "Randomized Sham Controlled Double-blind Trial of Repetitive Transcranial Magnetic Stimulation for Adults With Severe Tourette Syndrome". In: *Brain Stimulation* 8.3 (May 2015), pp. 574–581.

[46] Nudo, Randolph J. et al. "Neural Substrates for the Effects of Rehabilitative Training on Motor Recovery After Ischemic Infarct". In: *Science* 272.5269 (June 1996), pp. 1791–1794.

[47] Hoffman, D. S. and Strick, P. L. "Effects of a primary motor cortex lesion on step-tracking movements of the wrist". In: *Journal of Neurophysiology* 73.2 (Feb. 1995), pp. 891–895.

[48] Glees, P. and Cole, J. "Recovery Of Skilled Motor Functions After Small Repeated Lesions Of Motor Cortex In Macaque". In: *Journal of Neurophysiology* 13.2 (Mar. 1950), pp. 137–148.

[49] Pandarinath, Chethan et al. "Inferring single-trial neural population dynamics using sequential auto-encoders". In: *Nature Methods* 15.10 (Oct. 2018), pp. 805–815.

[50] Gilja, Vikash et al. "A high-performance neural prosthesis enabled by control algorithm design". In: *Nature Neuroscience* 15.12 (Dec. 2012).

[51] Krakauer, John W. et al. "Neuroscience Needs Behavior: Correcting a Reductionist Bias". In: *Neuron* 93.3 (Feb. 2017).

[52] Bialek, William. "On the dimensionality of behavior". In: *Proceedings of the National Academy of Sciences* 119.18 (May 2022).

[53] Nakagawa, Shinichi. "A farewell to Bonferroni: the problems of low statistical power and publication bias". In: *Behavioral Ecology* 15.6 (Nov. 2004).

[54] Noble, William S. "How does multiple testing correction work?" In: *Nature Biotechnology* 27.12 (Dec. 2009).

[55] Zeiler, Steven R et al. "Paradoxical Motor Recovery From a First Stroke After Induction of a Second Stroke: Reopening a Postischemic Sensitive Period". In: *Neurorehabilitation and neural repair* 30.8 (2016), pp. 794–800.

[56] Bray, IE, Clarke, SE, and Nuyujukian, P. "Neuroelectrophysiology-Compatible Electrolytic Lesioning". In: *eLife (under preprint review)* (2022).

[57] Nudo, R. J. et al. "A Squirrel Monkey Model of Poststroke Motor Recovery". In: *ILAR Journal* 44.2 (Jan. 2003), pp. 161–174.

[58] Wurtz, R H and Goldberg, M E. "Activity of superior colliculus in behaving monkey. IV. Effects of lesions on eye movements." In: *Journal of Neurophysiology* 35.4 (July 1972), pp. 587–596.

[59] Khateeb, Karam et al. "A versatile toolbox for studying cortical physiology in primates". In: *Cell Reports Methods* 2.3 (Mar. 2022), p. 100183.

[60] Balbi, Matilde et al. "Gamma frequency activation of inhibitory neurons in the acute phase after stroke attenuates vascular and behavioral dysfunction". In: *Cell Reports* 34.5 (Feb. 2021), p. 108696.

[61] Clark, Taylor A. et al. "Artery targeted photothrombosis widens the vascular penumbra, instigates peri-infarct neovascularization and models forelimb impairments". In: *Scientific Reports* 9.1 (Dec. 2019).

[62] Adkins-Muir, Deanna L. and Jones, Theresa A. "Cortical electrical stimulation combined with rehabilitative training: Enhanced functional recovery and dendritic plasticity following focal cortical ischemia in rats". In: *Neurological Research* 25.8 (Dec. 2003), pp. 780–788.

[63] Baron, Jean Claude et al. "Selective neuronal loss in ischemic stroke and cerebrovascular disease". In: *Journal of Cerebral Blood Flow and Metabolism* 34.1 (2014), pp. 2–18.

[64] Buzsáki, György. "Large-scale recording of neuronal ensembles". In: *Nature Neuroscience* 7.5 (May 2004), pp. 446–451.

[65] Nudo, Randolph J. "Recovery after brain injury: mechanisms and principles". In: *Frontiers in Human Neuroscience* 7 (2013).

[66] Park, Michael C. et al. "Consistent Features in the Forelimb Representation of Primary Motor Cortex in Rhesus Macaques". In: *The Journal of Neuroscience* 21.8 (Apr. 2001), pp. 2784–2792.

[67] Young, Nicole A., Collins, Christine E., and Kaas, Jon H. "Cell and neuron densities in the primary motor cortex of primates". In: *Frontiers in Neural Circuits* 7 (2013).

[68] Wood, Heather. "Selective neuronal loss could limit penumbral rescue after stroke". In: *Nature Reviews Neurology* 14.7 (July 2018).

[69] Morris, Rhiannon S. et al. "Relationships between selective neuronal loss and microglial activation after ischaemic stroke in man". In: *Brain* 141.7 (2018), pp. 2098–2111.

[70] Baron, Jean-Claude. "Protecting the ischaemic penumbra as an adjunct to thrombectomy for acute stroke". In: *Nature Reviews Neurology* 14.6 (June 2018).

[71] Veluw, Susanne J van et al. "Detection, risk factors, and functional consequences of cerebral microinfarcts". In: *The Lancet Neurology* 16.9 (Sept. 2017).

[72] Sobel, Raymond A. "Greenfield's Neuropathology, Ninth Edition: 2-Volume Set". In: *Journal of Neuropathology & Experimental Neurology* 74.12 (Dec. 2015), pp. 1185–1185.

[73] Ganguly, Karunesh et al. "Modulation of neural co-firing to enhance network transmission and improve motor function after stroke". In: *Neuron* 110.15 (Aug. 2022), pp. 2363–2385.

[74] Khanna, Preeya et al. "Low-frequency stimulation enhances ensemble co-firing and dexterity after stroke". In: *Cell* 184.4 (Feb. 2021).

[75] Kao, Jonathan C. et al. "Single-trial dynamics of motor cortex and their applications to brain-machine interfaces". In: *Nature Communications* 6.1 (Nov. 2015), p. 7759.

[76] Jolliffe, I.T. *Principal Component Analysis*. 2e. New York: Springer-Verlag, 2002.

[77] Sajid, Noor et al. "Degeneracy and Redundancy in Active Inference." In: *Cerebral cortex (New York, N.Y. : 1991)* 30.11 (2020), pp. 5750–5766.

[78] Hennig, Jay A et al. "Constraints on neural redundancy". In: *eLife* 7 (Aug. 2018).

[79] Churchland, Mark M et al. "Stimulus onset quenches neural variability: a widespread cortical phenomenon". In: *Nature Neuroscience* 13.3 (Mar. 2010), pp. 369–378.

[80] Sussillo, David. "Neural circuits as computational dynamical systems". In: *Current Opinion in Neurobiology* 25 (Apr. 2014), pp. 156–163.

[81] Eliasmith, Chris. "A Unified Approach to Building and Controlling Spiking Attractor Networks". In: *Neural Computation* 17.6 (June 2005), pp. 1276–1314.

[82] Bekolay, Trevor et al. "Nengo: a Python tool for building large-scale functional brain models". In: *Frontiers in Neuroinformatics* 7 (2014).

[83] Munafò, Marcus R. and Davey Smith, George. "Robust research needs many lines of evidence". In: *Nature* 553.7689 (Jan. 2018).

[84] Saxena, Shreya and Cunningham, John P. "Towards the neural population doctrine". In: *Current Opinion in Neurobiology* 55 (Apr. 2019), pp. 103–111.

[85] Xie, Yang et al. "Geometry of sequence working memory in macaque prefrontal cortex". In: *Science* 375.6581 (Feb. 2022), pp. 632–639.

[86] Harvey, Christopher D., Coen, Philip, and Tank, David W. "Choice-specific sequences in parietal cortex during a virtual-navigation decision task". In: *Nature* 484.7392 (Apr. 2012), pp. 62–68.

[87] Driscoll, Laura N. et al. "Dynamic Reorganization of Neuronal Activity Patterns in Parietal Cortex". In: *Cell* 170.5 (Aug. 2017), pp. 986–999.

[88] Gallego, Juan A. et al. "Neural Manifolds for the Control of Movement". In: *Neuron* 94.5 (June 2017), pp. 978–984.

[89] Gallego, Juan A. et al. "Long-term stability of cortical population dynamics underlying consistent behavior". In: *Nature Neuroscience* 23.2 (Feb. 2020), pp. 260–270.

[90] Gallego, Juan A. et al. "Cortical population activity within a preserved neural manifold underlies multiple motor behaviors". In: *Nature Communications* 9.1 (Dec. 2018), p. 4233.

[91] Hallinen, Kelsey M et al. "Decoding locomotion from population neural activity in moving C. elegans". In: *eLife* 10 (July 2021).

[92] Sussillo, David et al. "A neural network that finds a naturalistic solution for the production of muscle activity". In: *Nature Neuroscience* 18.7 (July 2015), pp. 1025–1033.

[93] Mante, Valerio et al. "Context-dependent computation by recurrent dynamics in prefrontal cortex". In: *Nature* 503.7474 (Nov. 2013), pp. 78–84.

[94] Kato, Saul et al. "Global Brain Dynamics Embed the Motor Command Sequence of Caenorhabditis elegans". In: *Cell* 163.3 (Oct. 2015).

[95] Lin, Qian et al. "Cerebellar Neurodynamics Predict Decision Timing and Outcome on the Single-Trial Level". In: *Cell* 180.3 (Feb. 2020), pp. 536–551.

[96] Nieh, Edward H. et al. "Geometry of abstract learned knowledge in the hippocampus". In: *Nature* 595.7865 (July 2021), pp. 80–84.

[97] Jonas, Eric and Kording, Konrad Paul. "Could a Neuroscientist Understand a Microprocessor?" In: *PLOS Computational Biology* 13.1 (Jan. 2017), e1005268.

[98] Kriegeskorte, Nikolaus and Wei, Xue-Xin. "Neural tuning and representational geometry". In: *Nature Reviews Neuroscience* 22.11 (Nov. 2021).

[99] Liu, Junjie V. et al. "Assessment of Stimulus-Induced Changes in Human V1 Visual Field Maps". In: *Journal of Neurophysiology* 96.6 (Dec. 2006), pp. 3398–3408.

[100] Aflalo, T. N. and Graziano, M. S. A. "Possible Origins of the Complex Topographic Organization of Motor Cortex: Reduction of a Multidimensional Space onto a Two-Dimensional Array". In: *Journal of Neuroscience* 26.23 (June 2006), pp. 6288–6297.

[101] Shkarina, Kateryna et al. "Optogenetic activators of apoptosis, necroptosis, and pyroptosis". In: *Journal of Cell Biology* 221.6 (June 2022).

[102] Smart, Ashley D. et al. "Engineering a light-activated caspase-3 for precise ablation of neurons in vivo". In: *Proceedings of the National Academy of Sciences* 114.39 (Sept. 2017).

[103] Marr, David. *Vision: A Computational Investigation into the Human Representation and Processing of Visual Information*. The MIT Press, 2010.

[104] Dubreuil, Alexis et al. "The role of population structure in computations through neural dynamics". In: *Nature Neuroscience* 25.6 (June 2022), pp. 783–794.

[105] Macpherson, Tom et al. "Natural and Artificial Intelligence: A brief introduction to the interplay between AI and neuroscience research". In: *Neural Networks* 144 (Dec. 2021), pp. 603–613.

[106] Barrett, David GT, Morcos, Ari S, and Macke, Jakob H. "Analyzing biological and artificial neural networks: challenges with opportunities for synergy?" In: *Current Opinion in Neurobiology* 55 (Apr. 2019), pp. 55–64.

[107] Hassabis, Demis et al. "Neuroscience-Inspired Artificial Intelligence". In: *Neuron* 95.2 (July 2017), pp. 245–258.

[108] Driscoll, Laura N., Duncker, Lea, and Harvey, Christopher D. "Representational drift: Emerging theories for continual learning and experimental future directions". In: *Current Opinion in Neurobiology* 76 (Oct. 2022), p. 102609.

[109] Hwang, Eun Jung et al. "Disengagement of motor cortex from movement control during long-term learning". In: *Science Advances* 5.10 (Oct. 2019).

[110] Darling, Warren G. et al. "Hand Motor Recovery Following Extensive Frontoparietal Cortical Injury Is Accompanied by Upregulated Corticoreticular Projections in Monkey". In: *The Journal of Neuroscience* 38.28 (July 2018), pp. 6323–6339.

[111] Tapia, Jesus A. et al. "The Existence of the StartReact Effect Implies Reticulospinal, Not Corticospinal, Inputs Dominate Drive to Motoneurons during Voluntary Movement". In: *The Journal of Neuroscience* 42.40 (Oct. 2022), pp. 7634–7647.

[112] DARLING, WARREN G., PIZZIMENTI, MARC A., and MORECRAFT, ROBERT J. "FUNCTIONAL RECOVERY FOLLOWING MOTOR CORTEX LESIONS IN NON-HUMAN PRIMATES: EXPERIMENTAL IMPLICATIONS FOR HUMAN STROKE PATIENTS". In: *Journal of Integrative Neuroscience* 10.03 (Sept. 2011), pp. 353–384.

[113] "Recommendations for Standards Regarding Preclinical Neuroprotective and Restorative Drug Development". In: *Stroke* 30.12 (Dec. 1999).

[114] National Research Council. *Guide for the Care and Use of Laboratory Animals*. 8th ed. 2011.

[115] Courtine, Grégoire et al. "Can experiments in nonhuman primates expedite the translation of treatments for spinal cord injury in humans?" In: *Nature Medicine* 13.5 (May 2007).

[116] Collinger, Jennifer L et al. "High-performance neuroprosthetic control by an individual with tetraplegia". In: *The Lancet* 381.9866 (Feb. 2013), pp. 557–564.

[117] Carrera, Emmanuel et al. "Is neural activation within the rescued penumbra impeded by selective neuronal loss?" In: *Brain* 136.6 (2013), pp. 1816–1829.

[118] Saver, Jeffrey L. "Time Is Brain—Quantified". In: *Stroke* 37.1 (Jan. 2006).

[119] Gomez, Camilo R. "Time Is Brain: The Stroke Theory of Relativity". In: *Journal of Stroke and Cerebrovascular Diseases* 27.8 (Aug. 2018), pp. 2214–2227.

[120] Lansberg, Maarten G et al. "MRI profile and response to endovascular reperfusion after stroke (DEFUSE 2): a prospective cohort study". In: *The Lancet Neurology* 11.10 (Oct. 2012).

[121] Wang, M. et al. "Cognitive Deficits and Delayed Neuronal Loss in a Mouse Model of Multiple Microinfarcts". In: *Journal of Neuroscience* 32.50 (Dec. 2012).

[122] Joy, Mary T. and Carmichael, S. Thomas. "Encouraging an excitable brain state: mechanisms of brain repair in stroke". In: *Nature Reviews Neuroscience* (Nov. 2020).

[123] Aswendt, Markus et al. "Lesion Size- and Location-Dependent Recruitment of Contralesional Thalamus and Motor Cortex Facilitates Recovery after Stroke in Mice". In: *Translational Stroke Research* (Mar. 2020).

[124] Chen, Chia-Ling et al. "Brain lesion size and location: Effects on motor recovery and functional outcome in stroke patients". In: *Archives of Physical Medicine and Rehabilitation* 81.4 (Apr. 2000), pp. 447–452.

[125] Kokinovic, Bojana and Medini, Paolo. "Loss of GABAB -mediated interhemispheric synaptic inhibition in stroke periphery". In: *The Journal of Physiology* 596.10 (May 2018).

[126] Wijngaarden, Joeri B. G. van et al. "The Impact of Cortical Lesions on Thalamo-Cortical Network Dynamics after Acute Ischaemic Stroke: A Combined Experimental and Theoretical Study". In: *PLOS Computational Biology* 12.8 (Aug. 2016), e1005048.

[127] Chen. "Distinct Inhibitory Circuits Orchestrate Cortical beta and gamma Band Oscillations". In: *Neuron* 96.6 (2017), pp. 1402–1418.

[128] Karvat, Golan, Alyahyay, Mansour, and Diester, Ilka. "Spontaneous activity competes with externally evoked responses in sensory cortex". In: *Proceedings of the National Academy of Sciences* 118.25 (June 2021), e2023286118.

[129] Telenczuk, Bartosz et al. "Local field potentials primarily reflect inhibitory neuron activity in human and monkey cortex". In: *Scientific Reports* 7.January (2017), pp. 1–10.

[130] Carson, Richard G. "Inter-hemispheric inhibition sculpts the output of neural circuits by co-opting the two cerebral hemispheres". In: *The Journal of Physiology* 598.21 (Nov. 2020).

[131] Zhang, Jing et al. "Local and large-scale beta oscillatory dysfunction in males with mild traumatic brain injury". In: *Journal of Neurophysiology* 124.6 (Dec. 2020), pp. 1948–1958.

[132] Kehnemouyi, Yasmine M et al. "Modulation of beta bursts in subthalamic sensorimotor circuits predicts improvement in bradykinesia". In: *Brain* 144.2 (Mar. 2021), pp. 473–486.

[133] Rule, Michael E, O'Leary, Timothy, and Harvey, Christopher D. "Causes and consequences of representational drift". In: *Current Opinion in Neurobiology* 58 (Oct. 2019), pp. 141–147.

[134] Schoonover, Carl E. et al. "Representational drift in primary olfactory cortex". In: *Nature* 594.7864 (June 2021), pp. 541–546.

[135] Marks, Tyler D. and Goard, Michael J. "Stimulus-dependent representational drift in primary visual cortex". In: *Nature Communications* 12.1 (Dec. 2021), p. 5169.

[136] Deitch, Daniel, Rubin, Alon, and Ziv, Yaniv. "Representational drift in the mouse visual cortex". In: *Current Biology* 31.19 (Oct. 2021), pp. 4327–4339.

[137] Murata, Y. et al. "Temporal Plasticity Involved in Recovery from Manual Dexterity Deficit after Motor Cortex Lesion in Macaque Monkeys". In: *Journal of Neuroscience* 35.1 (Jan. 2015).

[138] Moreau-Debord, Ian et al. "Rapid and bihemispheric reorganization of neuronal activity in premotor cortex after brain injury". In: *The Journal of Neuroscience* (Sept. 2021).

[139] Hordacre, Brenton et al. "Evidence for a Window of Enhanced Plasticity in the Human Motor Cortex Following Ischemic Stroke". In: *Neurorehabilitation and Neural Repair* 35.4 (Apr. 2021), pp. 307–320.

[140] Silasi, Gergely and Murphy, Timothy H. "Stroke and the Connectome: How Connectivity Guides Therapeutic Intervention". In: *Neuron* 83.6 (Sept. 2014).

[141] Jaillard, Assia et al. "Vicarious function within the human primary motor cortex?" In: *Brain* 128.5 (May 2005), pp. 1122–1138.

[142] Hahamy, Avital and Makin, Tamar R. "Remapping in Cerebral and Cerebellar Cortices Is Not Restricted by Somatotopy". In: *The Journal of Neuroscience* 39.47 (Nov. 2019), pp. 9328–9342.

[143] Jones, Theresa A. "Motor compensation and its effects on neural reorganization after stroke". In: *Nature Reviews Neuroscience* 18.5 (May 2017), pp. 267–280.

[144] Zeiger, William A. et al. "Barrel cortex plasticity after photothrombotic stroke involves potentiating responses of pre-existing circuits but not functional remapping to new circuits". In: *Nature Communications* 12.1 (Dec. 2021).

[145] Barrett, David GT, Denève, Sophie, and Machens, Christian K. "Optimal compensation for neuron loss". In: *eLife* 5 (Dec. 2016).

[146] Moore, Alexandra K. et al. "Rapid Rebalancing of Excitation and Inhibition by Cortical Circuitry". In: *Neuron* 97.6 (Mar. 2018), pp. 1341–1355.

[147] Di Pino, Giovanni et al. "Modulation of brain plasticity in stroke: A novel model for neurorehabilitation". In: *Nature Reviews Neurology* 10.10 (2014), pp. 597–608.

[148] Boddington, L. J. and Reynolds, J. N.J. "Targeting interhemispheric inhibition with neuromodulation to enhance stroke rehabilitation". In: *Brain Stimulation* 10.2 (2017), pp. 214–222.

[149] Khanna, Preeya and Carmena, Jose M. "Beta band oscillations in motor cortex reflect neural population signals that delay movement onset". In: (2017).

[150] Hwang, Fuu-Jiun et al. "Motor learning selectively strengthens cortical and striatal synapses of motor engram neurons". In: *Neuron* (July 2022).

[151] Zeiler, Steven R. and Krakauer, John W. "The interaction between training and plasticity in the poststroke brain". In: *Current Opinion in Neurology* 26.6 (Dec. 2013).

[152] Hennig, Jay A. et al. "Learning is shaped by abrupt changes in neural engagement". In: *Nature Neuroscience* 24.5 (May 2021).

[153] Hennig, Jay A. et al. "How learning unfolds in the brain: toward an optimization view". In: *Neuron* (Oct. 2021).

[154] Braun, D. A. et al. "Learning Optimal Adaptation Strategies in Unpredictable Motor Tasks". In: *Journal of Neuroscience* 29.20 (May 2009), pp. 6472–6478.

[155] Price, Cathy J and Friston, Karl J. "Degeneracy and cognitive anatomy". In: *Trends in Cognitive Sciences* 6.10 (Oct. 2002).

[156] Isomura, Takuya, Shimazaki, Hideaki, and Friston, Karl J. "Canonical neural networks perform active inference". In: *Communications Biology* 5.1 (Dec. 2022), p. 55.

[157] Mehrotra, Pavan et al. "An open-source realtime computational platform (short WIP paper)". In: *Proceedings of the 19th ACM SIGPLAN/SIGBED International Conference on Languages, Compilers, and Tools for Embedded Systems*. New York, NY, USA: ACM, June 2018, pp. 109–112.

[158] Chestek, Cynthia A et al. "Long-term stability of neural prosthetic control signals from silicon cortical arrays in rhesus macaque motor cortex". In: *Journal of Neural Engineering* 8.4 (Aug. 2011), p. 045005.

[159] Bean, Bruce P. "The action potential in mammalian central neurons". In: *Nature Reviews Neuroscience* 8.6 (June 2007), pp. 451–465.

[160] Bishop, C. M. and Nasrabadi, N. M. *Pattern Recognition and Machine Learning*. Vol. 4. New York: Springer-Verlag, 2006.

[161] Thevenaz, P., Ruttimann, U.E., and Unser, M. "A pyramid approach to subpixel registration based on intensity". In: *IEEE Transactions on Image Processing* 7.1 (1998), pp. 27–41.

[162] Maynard, Edwin M., Nordhausen, Craig T., and Normann, Richard A. "The Utah Intracortical Electrode Array: A recording structure for potential brain-computer interfaces". In: *Electroencephalography and Clinical Neurophysiology* 102.3 (Mar. 1997), pp. 228–239.

[163] Stringer, Carsen et al. "High-dimensional geometry of population responses in visual cortex". In: *Nature* 571.7765 (July 2019), pp. 361–365.

Supplementary Information: A low-dimensional biomarker of brain injury and behavior

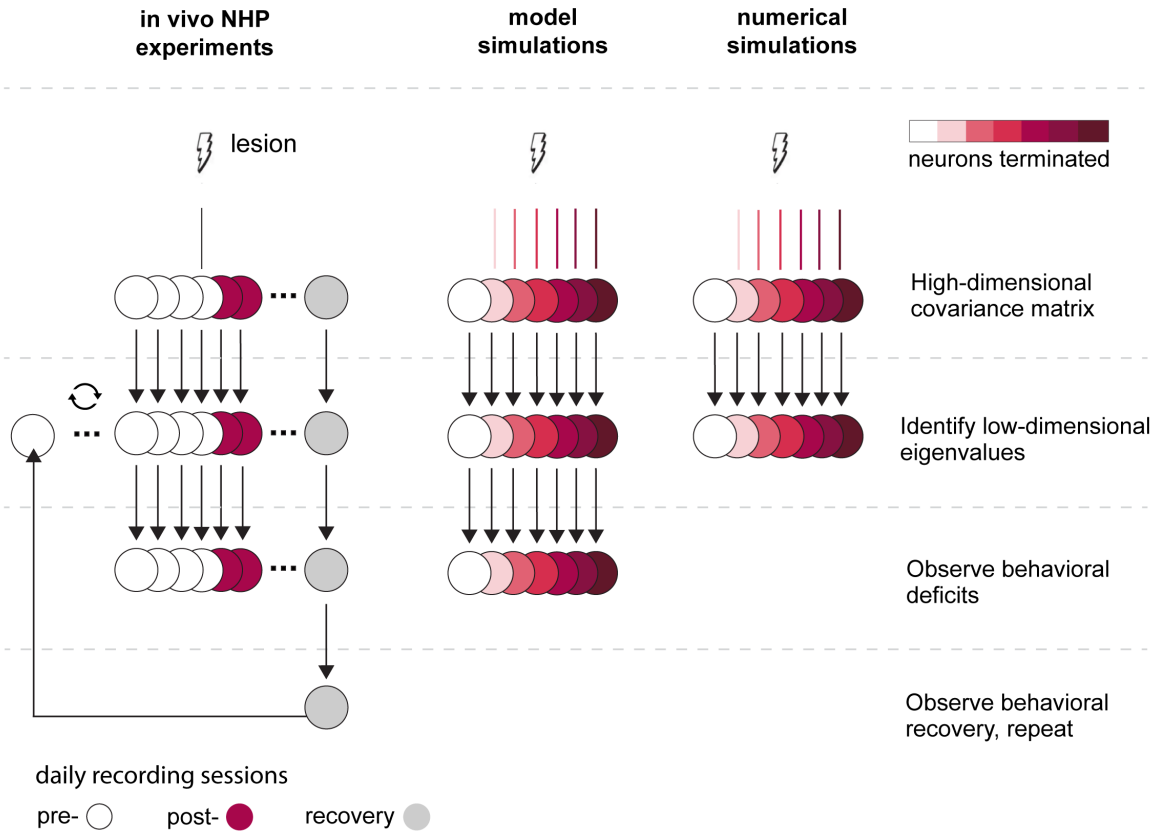

Figure S1:

Three approaches to study the impact of neuron loss on correlated neuron population activity. Spiking neural networks and numerical simulations were used to confirm properties of neuron loss observed during *in vivo* experiments (Figure 3 and Supplementary Figures S11-S14). The supporting evidence from these approaches provides further confidence in the results and helps to reduce and refine non-human primate experiments. *Numerical Simulations*: Random covariance matrices, imprinted with empirical correlation structure measured *in vivo*, were used to analyze neuron loss. These simulations represented pair-wise correlated activity between the neurons recorded by the 96 electrodes of a standard Utah array, allowing us to simulate thousands of "neuron" deletions and observe the effect on the correlation structure. The results provide a potential method to estimate neuron loss *in vivo*, which is presented in Supplementary Figures S13 and S14 and tested on a spiking neural network model. *Spiking Neural Network Simulations*: A similar approach was taken using a spiking neural network model, but here neurons in a trained network were randomly terminated and the covariance matrices were determined from the actual population spiking activity. Importantly, the task performance of the network provided a simple behavior that is a causal function of the model neurons' spiking activity. *In vivo Non-Human Primate Experiments*: Unlike simulations, adaptation of the recorded neuron population and natural recovery of behavior can be observed *in vivo*. Small lesions in primate motor cortex through chronically implanted electrode arrays reveal a continuum of recovery states over time that reflect varying degrees of network damage and behavioral performance. Notably, these surgery-free perturbations only affect precise task behaviors without affecting the animal's overall

well-being. Repetition of the controlled lesion procedure generated unique performance deficits with varied recovery timelines (Figure 1 and Supplementary Figure S2. Thus, the technique presented in this article provides an essential source of controlled randomization for uncovering causal brain-behavior relationships.[27,51]

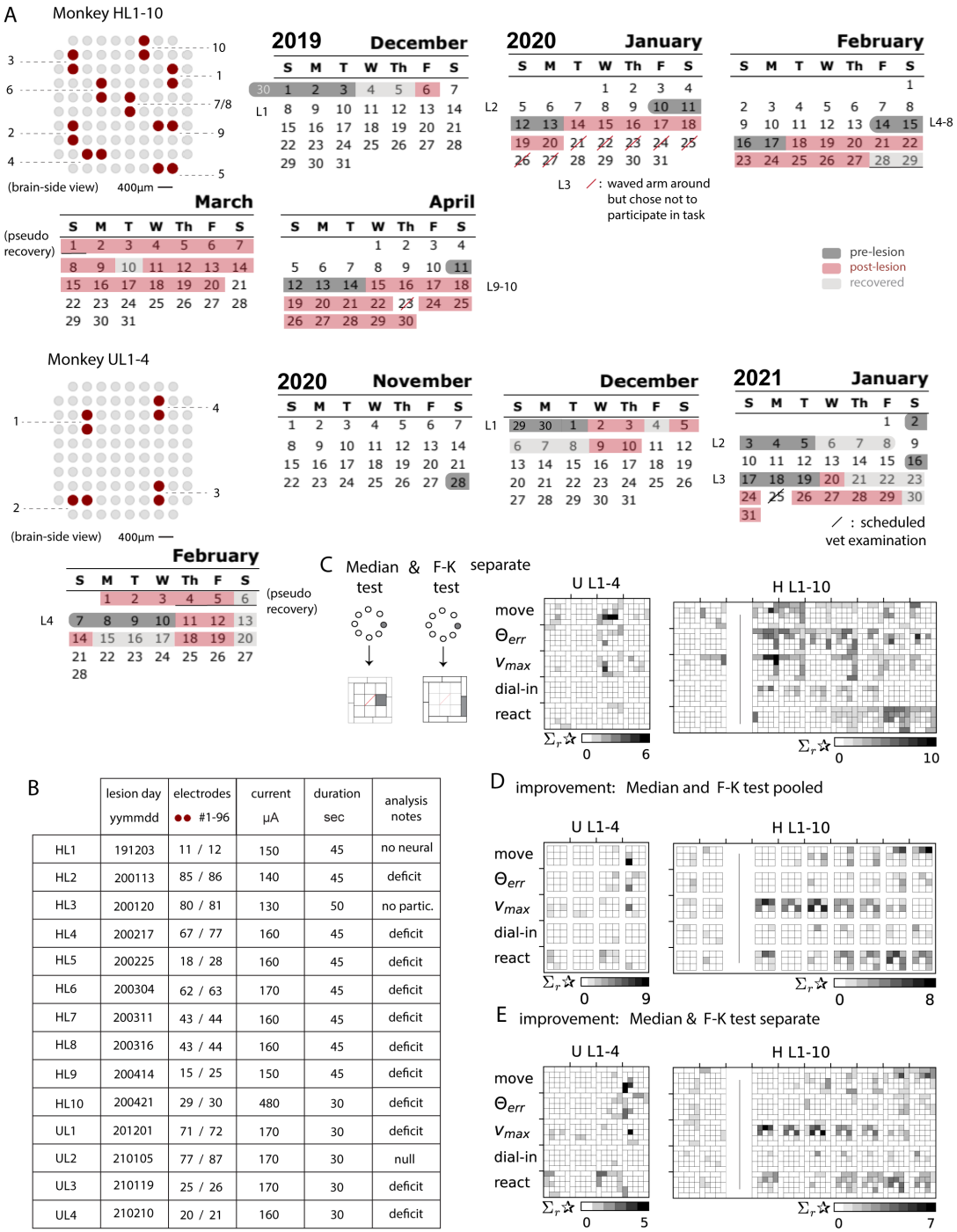

B

	lesion day yymmdd	electrodes ●● #1-96	current μA	duration sec	analysis notes
HL1	191203	11 / 12	150	45	no neural
HL2	200113	85 / 86	140	45	deficit
HL3	200120	80 / 81	130	50	no partic.
HL4	200217	67 / 77	160	45	deficit
HL5	200225	18 / 28	160	45	deficit
HL6	200304	62 / 63	170	45	deficit
HL7	200311	43 / 44	160	45	deficit
HL8	200316	43 / 44	160	45	deficit
HL9	200414	15 / 25	150	45	deficit
HL10	200421	29 / 30	480	30	deficit
UL1	201201	71 / 72	170	30	deficit
UL2	210105	77 / 87	170	30	null
UL3	210119	25 / 26	170	30	deficit
UL4	210210	20 / 21	160	30	deficit

Figure S2:

(a,b) Time course and parameters for all 14 electrolytic lesions. The experimental timeline shows deficit and recovery were not always cleanly separated, which is why lesions HL4-8 and H9-10, were grouped for subsequent analysis. c) Figure 1e in the main text shows pooled significance counts across both statistical tests; here the same data is broken down further by the median test and Fligner-Kileen's test, shown on the inner grid and outer ring respectively. Although not necessarily independent, it was common for only one of the tests to be affected for a given measure. d) Summary of detected improvements relative to pre-lesion data. These occurred in both the post-lesion and recovered groups. e) Significance counts for improvement, broken down further by statistical test.

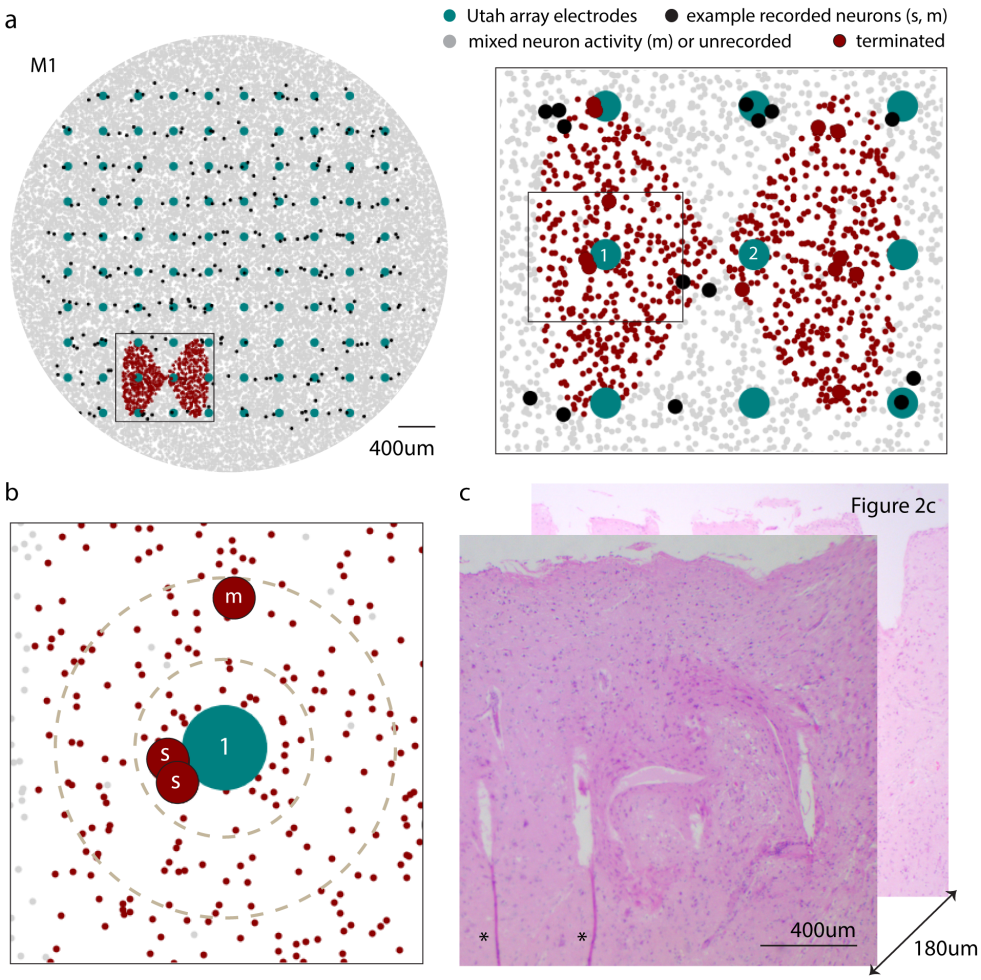

Figure S3:

Dense motor cortex population recordings and neuron loss. a) Neurons are represented as grey dots in a simulated patch of motor cortex (neurons at 0.1X their typical size); they were randomly distributed with a density determined by literature estimates of 50,000 neurons per mm^2 of flattened macaque cortex.[67] This density was divided by three since our recordings and lesion were largely contained to layers 2 and 3 of the six layered cortex, then further decreased 10-fold for visual clarity. The 96 recording electrodes of a conventional Utah array are shown in teal (2X scale) and nearby neurons "recorded" by the array were simulated and shown in black (4X scale). One to five examples of recorded neurons were randomly highlighted for each electrode, determined by draws from a binomial distribution (n=5, p=0.6). These neurons were located a random distance away, determined by draws from a normal distribution centered on the specified electrode's position, with a standard deviation of 0.05mm. This gave just short of 300 recorded neurons for the entire array, reflecting the spiking activity of both isolated single neurons (s), found 30-70µm from the electrode tip,[162] as well as the multi-unit spiking activity from many additional nearby neurons[64] (m), found within a known recording radius of approximately 150µm. Note, only a tiny fraction of the local population is recorded, and an even smaller fraction are neurons that can be truly isolated. A lesion of comparable size and shape to the in vivo experiments was then simulated around two electrodes, labelled 1 and 2. An exaggerated 90% of all neurons within the entire lesion boundary were randomly terminated (set to dark red). b) Close-up of a lesion electrode. While most of the recorded neurons and background neurons were

terminated, a few neurons are likely to survive in the mixed-neuron recording volume for each electrode (in this case, four). Note that our under-representation of neuron density directly underestimates this count. The mixed spiking activity of the nearby neurons can still be be recorded and may not show much change in the averaged waveform observed before a lesion. c) We also hypothesize that we are able to continue to record neurons on all 96 electrodes since the ablated and necrotic zones are not entirely homogeneous (cannot be seen in Figure 2). It is also worth noting that the axial plane of the lesion does not lay parallel with the surface of the array or the brain; in some cases, the ablation projected out from the tip of the electrode, leaving spared neurons lying just above (e.g., Figure 2c), whereas in other cases the ablation and heat necrosis regions occur slightly higher up the electrode shaft, leaving viable tissue below the tip. In the example H&E stained slice shown here, there appears to be partially damaged tissue that extends into the lesion core in Figure 2a. These two example slices are separated by 180μm, illustrating the degree to which the injury changes over relatively small distances. The color streaks labeled by the asterisks are tissue folds caused by mounting the tissue slice, and not the result of the lesion.

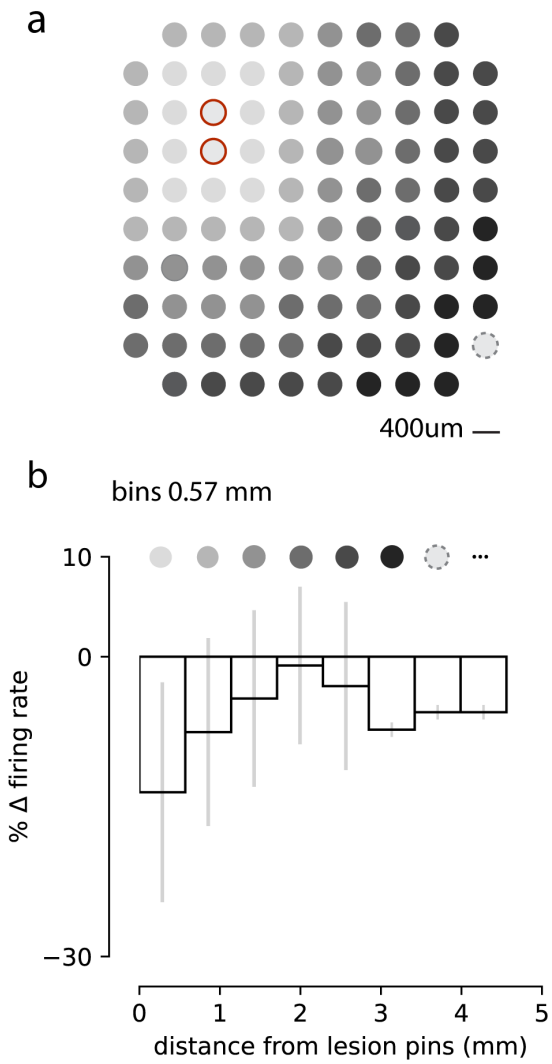

Figure S4:

Acute post-lesion change in spike counts as a function of distance from the lesion electrodes. a) Discrete bins were constructed to smooth out the unevenly spaced set of distances $\sqrt{(0.4n_x)^2 + (0.4n_y)^2}$mm, where $n_{x,y}$ are the number of electrodes from the nearest lesion electrode in the horizontal and vertical direction, respectively. A bin size of 0.57mm was chosen as the minimum resolution that would include all contiguous electrodes found around the two lesion electrodes; these groupings are illustrated for UL1 on the 96-electrode Utah array. b) The exact distribution shape depended on the selection of bin size, but a general trend holds: the median percent change in electrode-specific spike counts occurring during the peri-move period, [-50,400]ms, decreased during an acute post-lesion period, days [1, 2, 3], when compared pairwise to the pre-lesion days [-3,-2,-1,0]. The standard error associated with each group is illustrated in grey, highlighting the variable patterns of individual neurons' increases and decreases of activity within each distance group. Note that activity changes were observed across the array at distances that exceed the focal lesion size identified visually (Figure 2), likely reflecting both remote neuron loss and broader network adaptation.

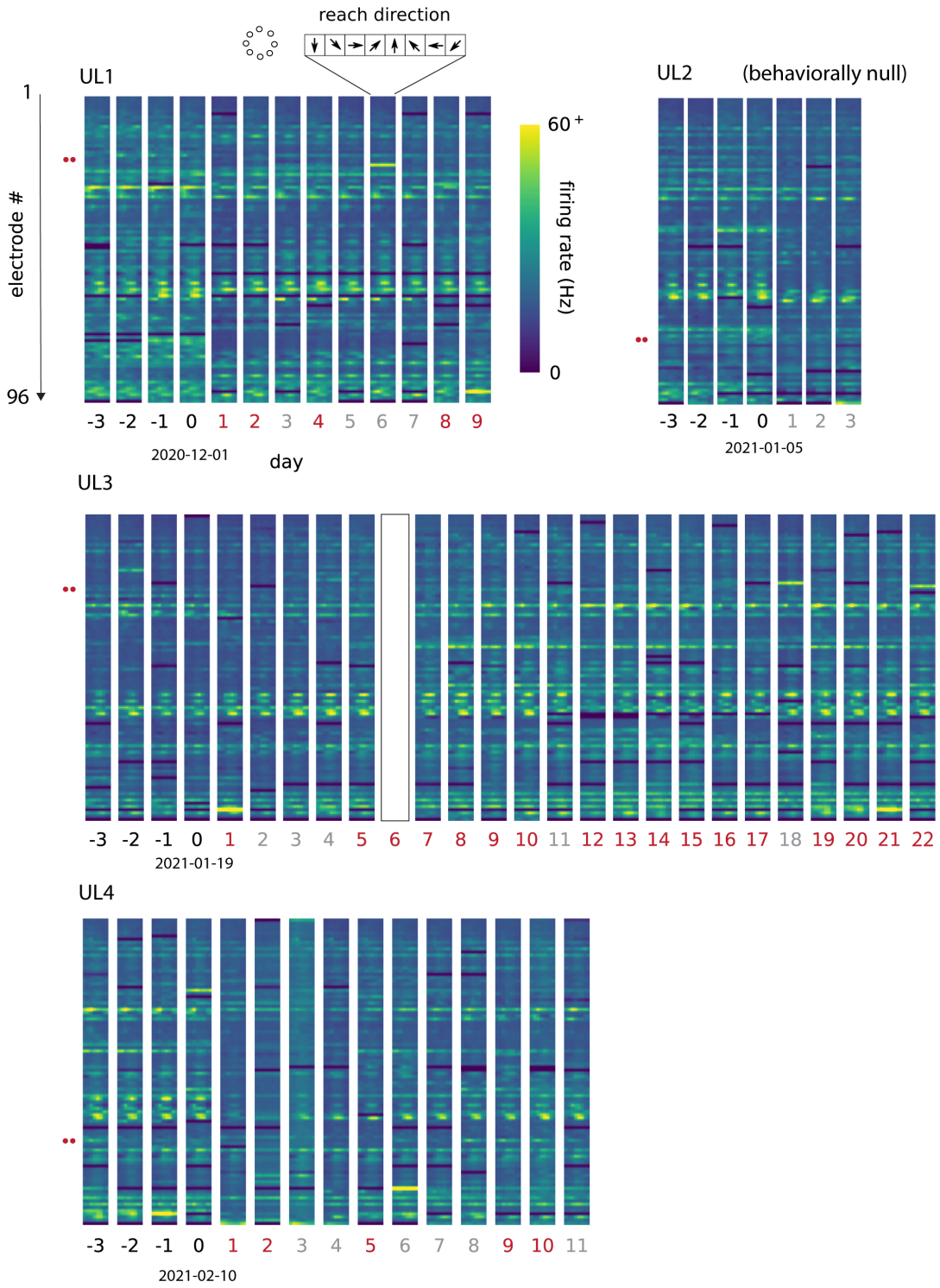

Figure S5:

Electrolytic lesions affect single neuron tuning (Monkey U). Spike counts were computed for each electrode during the peri-move period of the reach [-50,400]ms. This set of successful reach trials was broken down by target and presented as median firing rates for each electrode. Changes in firing rate and preferred directional tuning can be observed across the 4x4mm^2 array, both proximal and distal from the lesion electrodes (location marked by red dots).

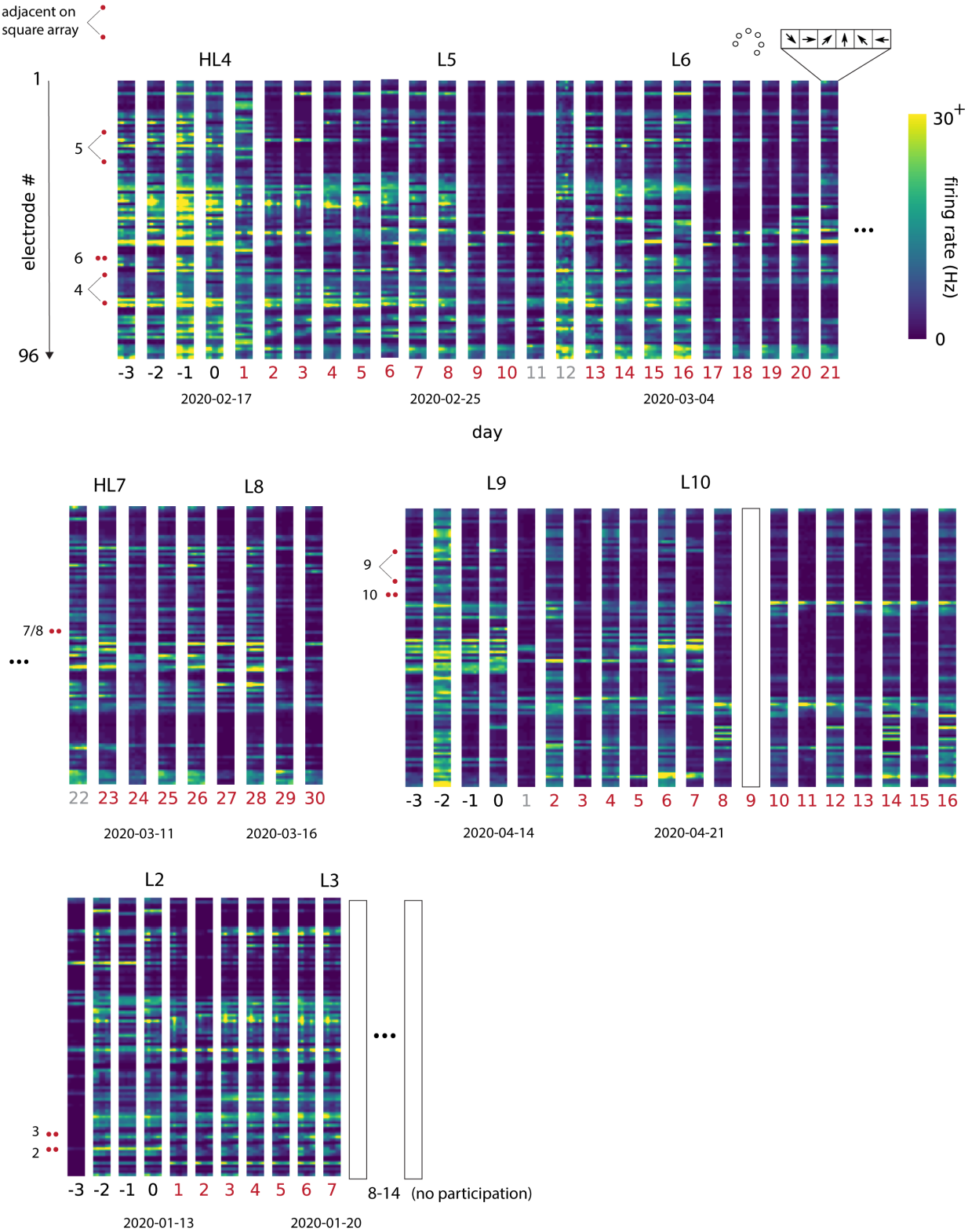

Figure S6:

Electrolytic lesions affect single neuron tuning (Monkey H). Only six of eight targets were presented to Monkey H due to a visual field deficit.

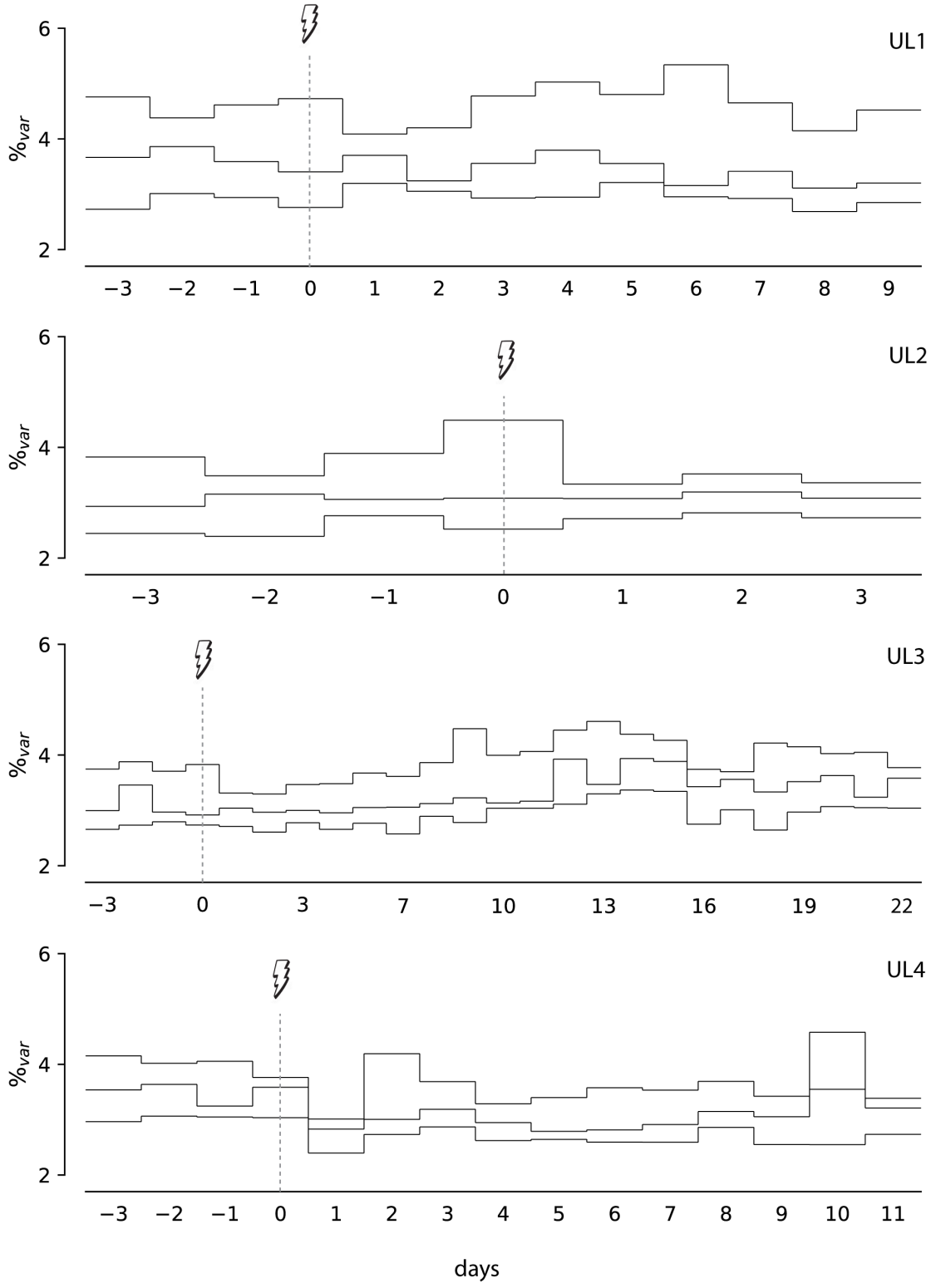

Figure S7:

Daily timecourse of population covariance matrix eigenvalues, before and after a lesion (Monkey U). Eigenvalue magnitude is expressed as percentage of the total explained variance.

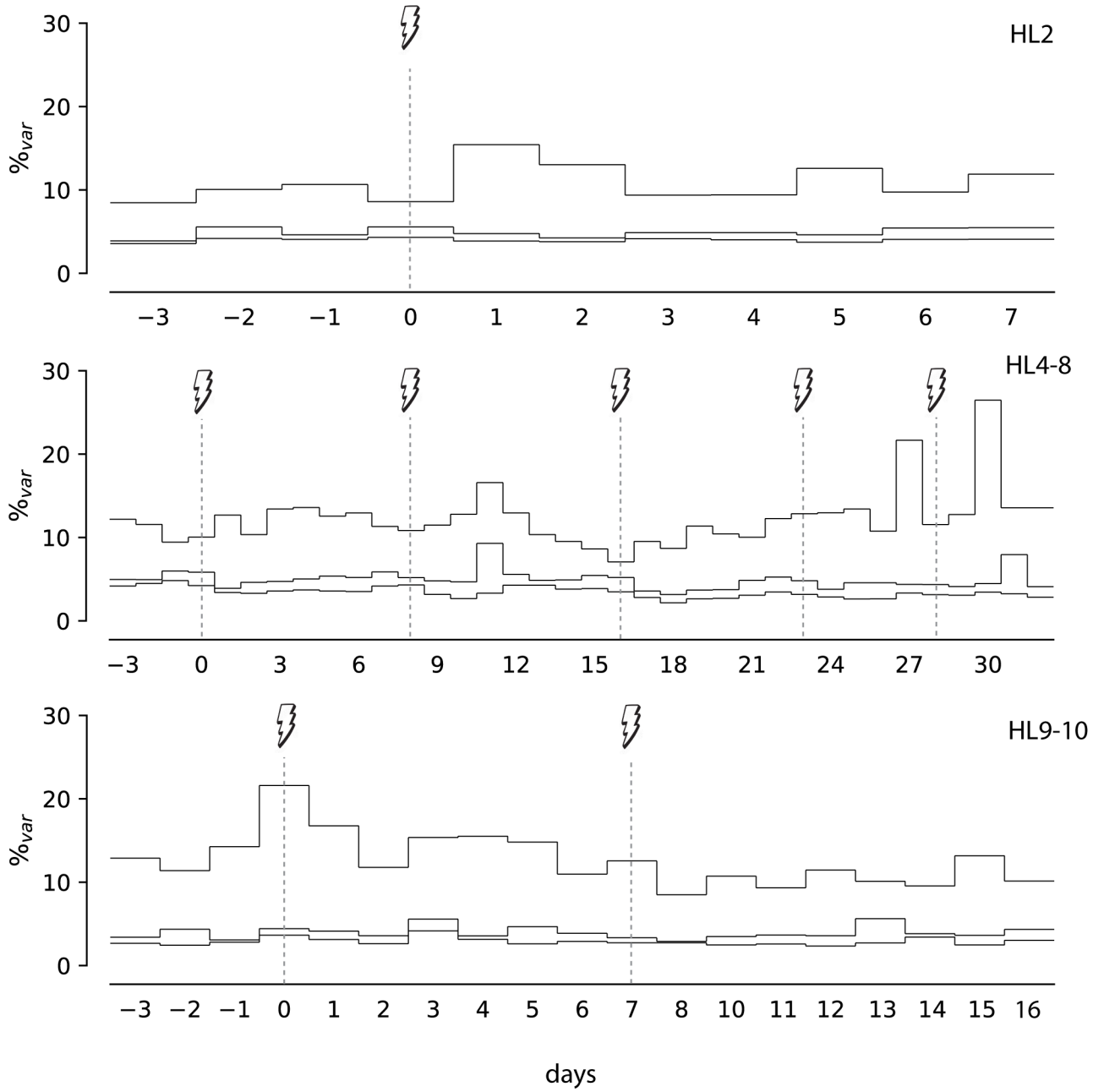

Figure S8:

Daily timecourse of population covariance matrix eigenvalues, before and after a lesion (Monkey H).

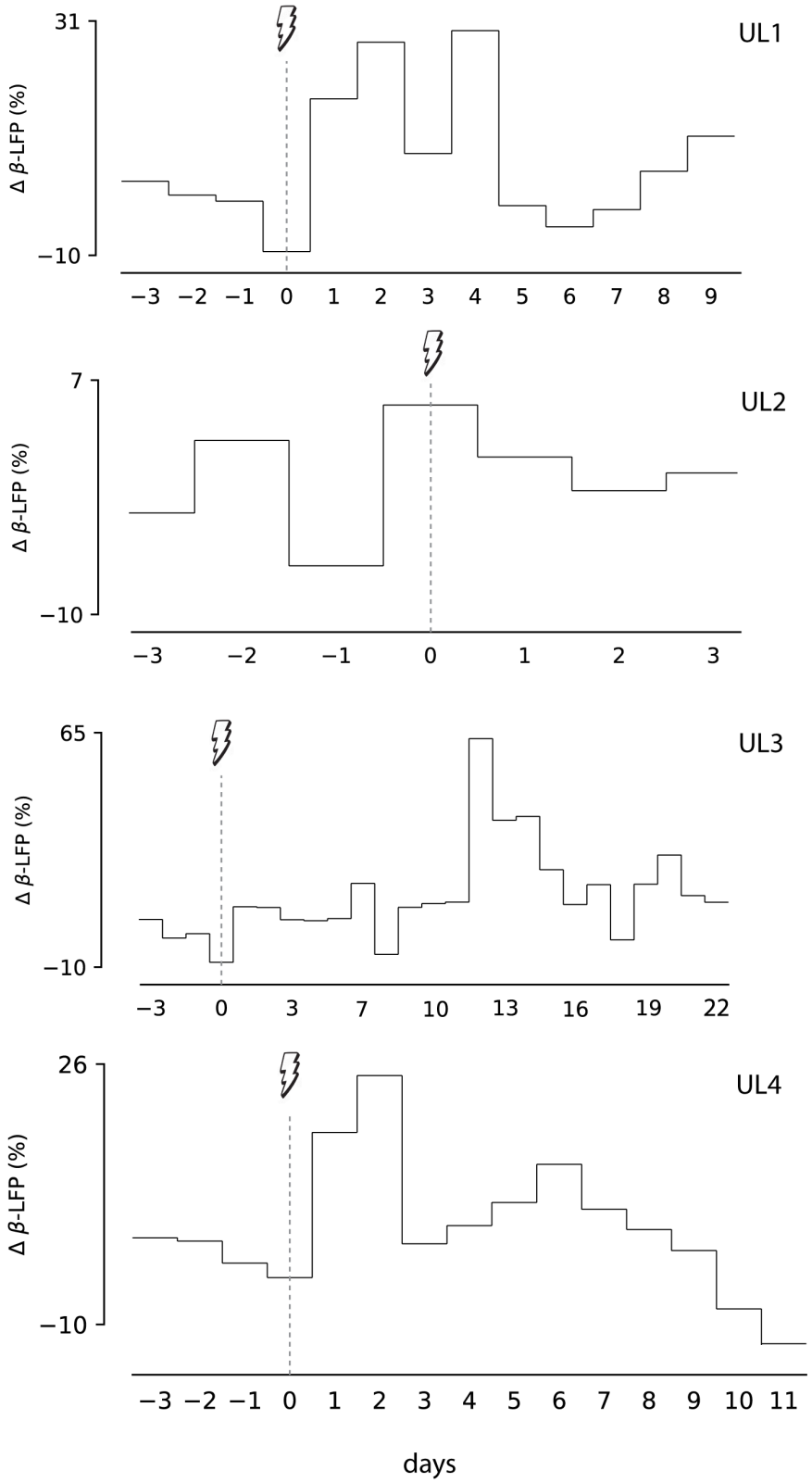

Figure S9:

Daily timecourse of the percent change in peri-move β- power, measured across the array before and after a lesion (Monkey U).

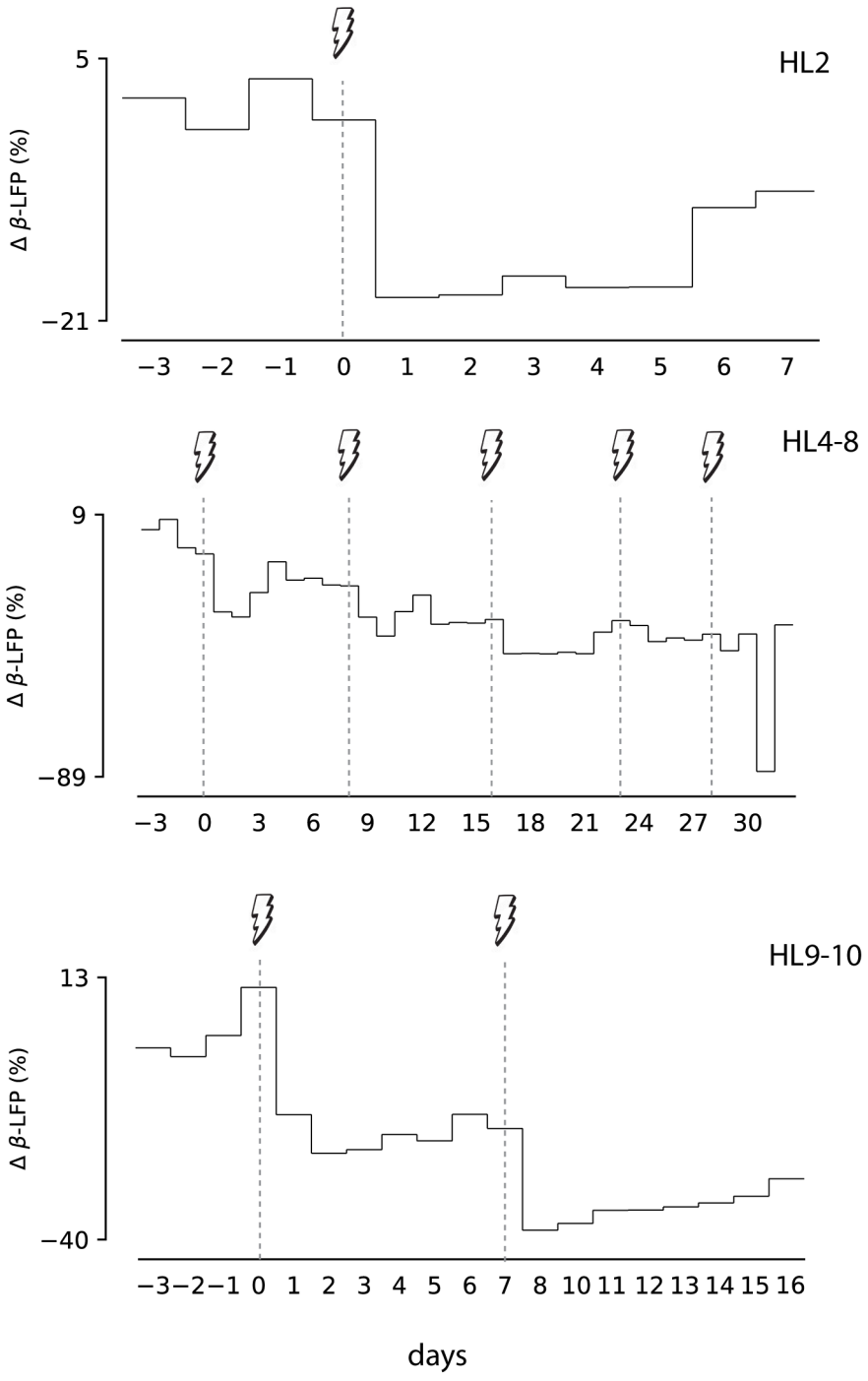

Figure S10:

Daily timecourse of the percent change in peri-move β-LFP power, measured across the array before and after a lesion (Monkey H).

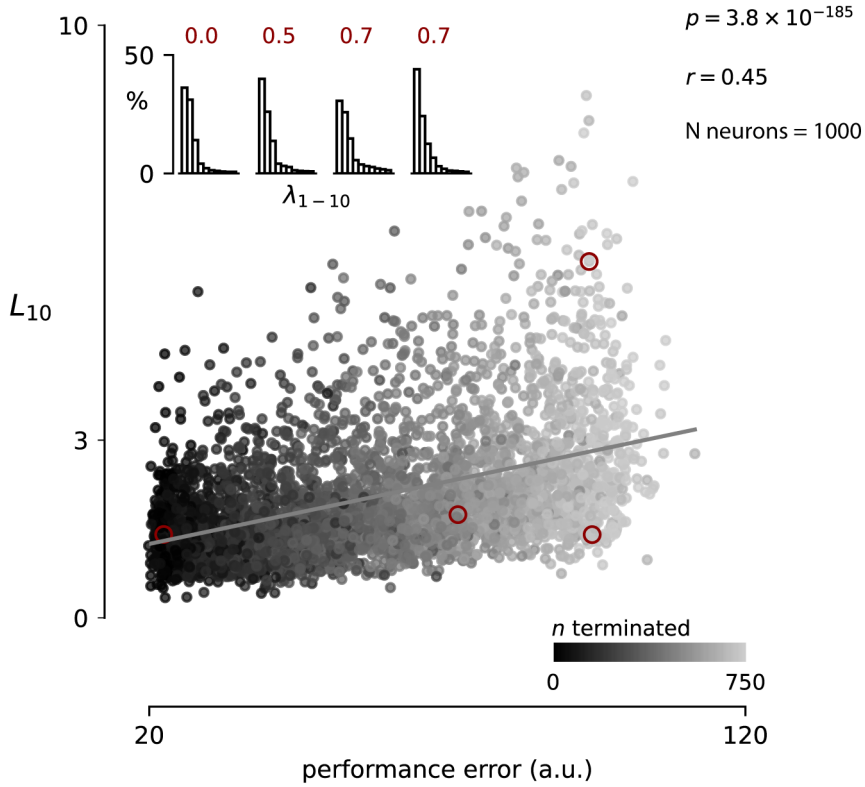

Figure S11:

Termination of neurons in a spiking neural network model recapitulated the experimental results. A spiking neural network model composed of 1000 leaky-integrate and fire neurons was constructed by finding synaptic weights that produce integrator dynamics[81,82] like those displayed in motor cortex. While any of the 1000 model neurons could be deleted for a specific lesion simulation, only 96 of the 1000 were randomly selected to mimic a noisy sample recording from the population. The network was presented a one-dimensional piece-wise linear input signal, which was reproduced as output. The difference between the input and output was calculated as a residual sum of squares (performance error) and serves as a proxy for behavioral performance that is regressed against the value of L_{10}. The grey-scale shading indicates the fraction of terminated neurons. The effects of termination on the contributions of the top ten eigenvalues are illustrated for four example deletions (inset histograms, scatter points circled in red). These histograms capture some of the typical changes seen in vivo, where the relative contributions of the largest sample eigenvalues can either increase or decrease as a result of neuron loss. The model confirms the basic intuition that the relative changes within these largest eigenvalues and the extent of behavioral deficit directly correlate with the severity of the brain injury (number of neurons terminated).

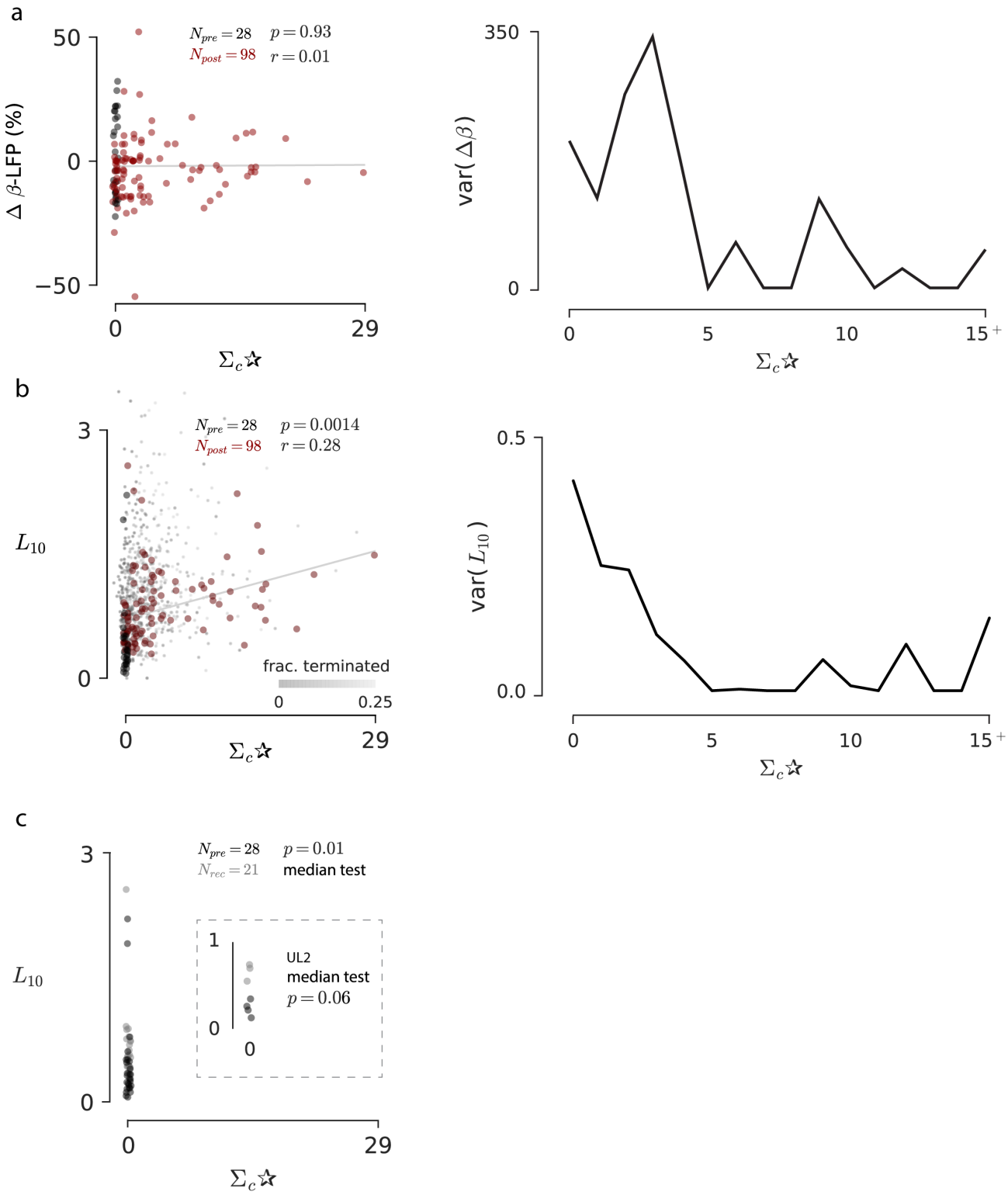

Figure S12:

a) The change in β-LFP power during movement as a function of the total daily behavioral deficit, including seven outliers that fell above the 95th percentile (excluded in main text; Figure 3c). The vari-

ance of $\Delta\beta$ tended to decrease as a function of behavioral deficit and more severe injury. Considering the absolute value of the change of β-LFP power was also not significant. b) *Left* The biomarker L_{10}, including the seven outliers excluded from Figure 3d. The rationale for treating these as outliers is as follows: a large neuron population perturbation within a given recorded sample of motor cortex without any palpable behavioral impairment and continuity across daily recording sessions is easily identified. Note that the network model (small grey scale dots) also shows these infrequent, large excursions in L_{10} when impairment is minimal and network simulations have experienced little-to-no neuron loss. Given the largest lesion was estimated to remove about 25% of local neurons, only simulations with a terminated fraction of 0-0.25 were plotted. For direct comparison, the behavioral performance axis of the model (arbitrary units) was scaled to the behavioral deficit axis from the in vivo experiments 3. *Right* As observed for the local field potential, the variance of the *in vivo* biomarker was high for small behavioral deficits but quickly decreased for larger deficits, roughly corresponding to larger proportions of neuron loss (inferred from model simulations, see Figure S11). These results are likely explained by the under-sampling of the true population and representational drift (degeneracy) in motor cortex, where many patterns of high dimensional activity can manifest similarly in the population activity and drive the same behavior. Injury conditions that lead to more pronounced behavioral deficits appear to constrain the system's ability to fully utilize the activity space, which quenches the variability of the sampled network. This variability quenching is a well known phenomena that can result from input-driven activation states in various regions of cortex.[79] c) The L_{10} biomarker (including outliers) nearly returns to pre-lesion levels on recovered behavioral days. The median test suggests a slight but significant rise in L_{10} for all the recovered days with respect to pre-lesion variability ($p = 0.01$). The null lesion in Monkey U (L2) showed no significant behavioral deficit and L_{10} was not significantly different when compared to the entire pre-lesion set, as well as just the UL2 pre-lesion days (median test, $p = 0.2$ and $p = 0.06$, inset). Despite the obvious decrease in variability for UL2 post-days (1, 2 and 3; see Supplementary Figure S7), the change from median pre-lesion λ_k values were small. Overall there was a close match between the biomarker measured on pre-lesion days and behaviorally normal post-lesion days.

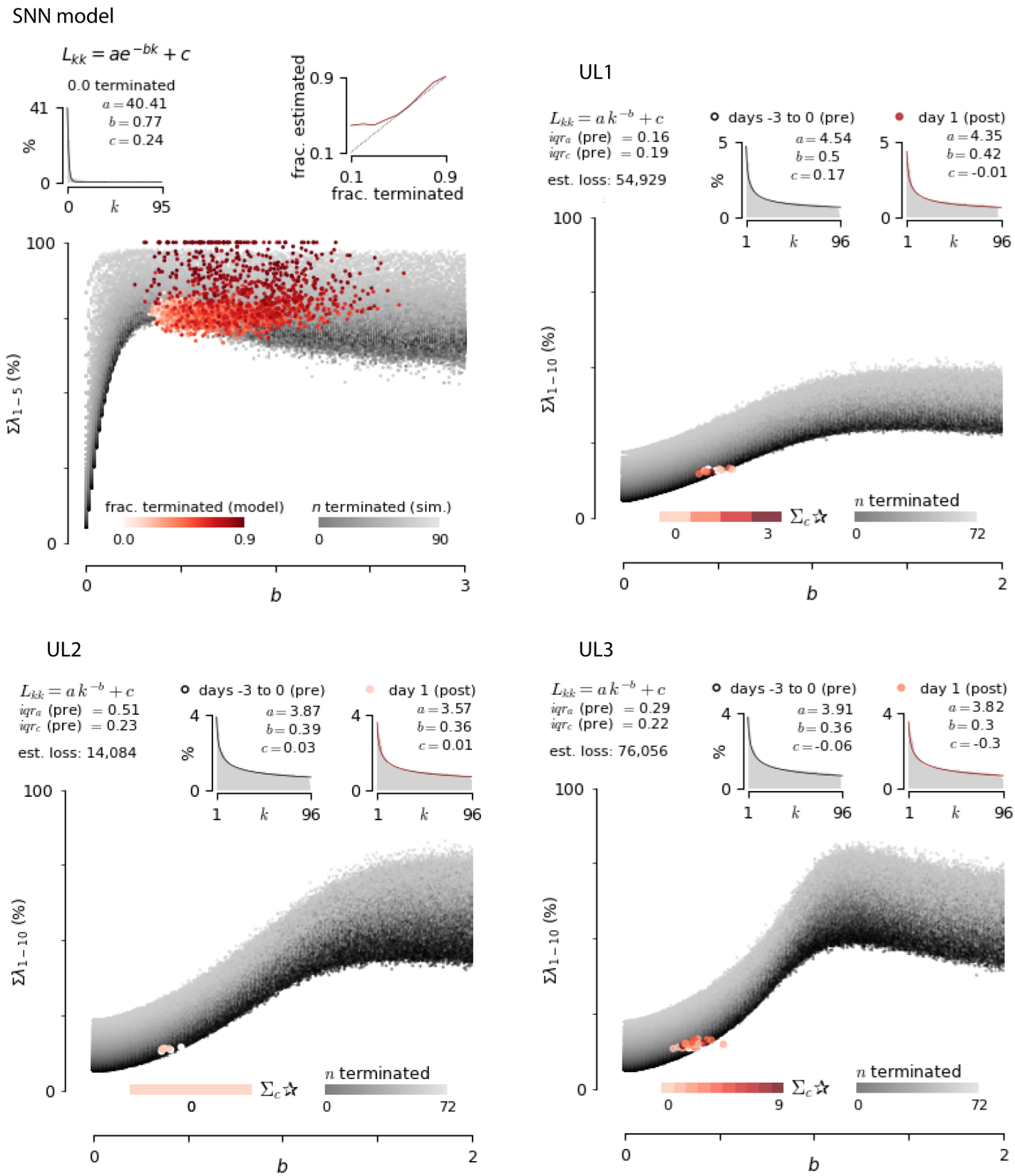
SNN model
$L_{kk} = ae^{-bk} + c$
0.0 terminated
$a = 40.41$
$b = 0.77$
$c = 0.24$
frac. estimated
frac. terminated
$\Sigma\lambda_{1-5}$ (%)
frac. terminated (model)
n terminated (sim.)
UL1
$L_{kk} = a\,k^{-b} + c$
iqr_a (pre) = 0.16
iqr_c (pre) = 0.19
est. loss: 54,929
days -3 to 0 (pre)
day 1 (post)
$a = 4.54$
$b = 0.5$
$c = 0.17$
$a = 4.35$
$b = 0.42$
$c = -0.01$
$\Sigma\lambda_{1-10}$ (%)
n terminated
UL2
$L_{kk} = a\,k^{-b} + c$
iqr_a (pre) = 0.51
iqr_c (pre) = 0.23
est. loss: 14,084
days -3 to 0 (pre)
day 1 (post)
$a = 3.87$
$b = 0.39$
$c = 0.03$
$a = 3.57$
$b = 0.36$
$c = 0.01$
$\Sigma\lambda_{1-10}$ (%)
n terminated
UL3
$L_{kk} = a\,k^{-b} + c$
iqr_a (pre) = 0.29
iqr_c (pre) = 0.22
est. loss: 76,056
days -3 to 0 (pre)
day 1 (post)
$a = 3.91$
$b = 0.36$
$c = -0.06$
$a = 3.82$
$b = 0.3$
$c = -0.3$
$\Sigma\lambda_{1-10}$ (%)
n terminated

Figure S13:

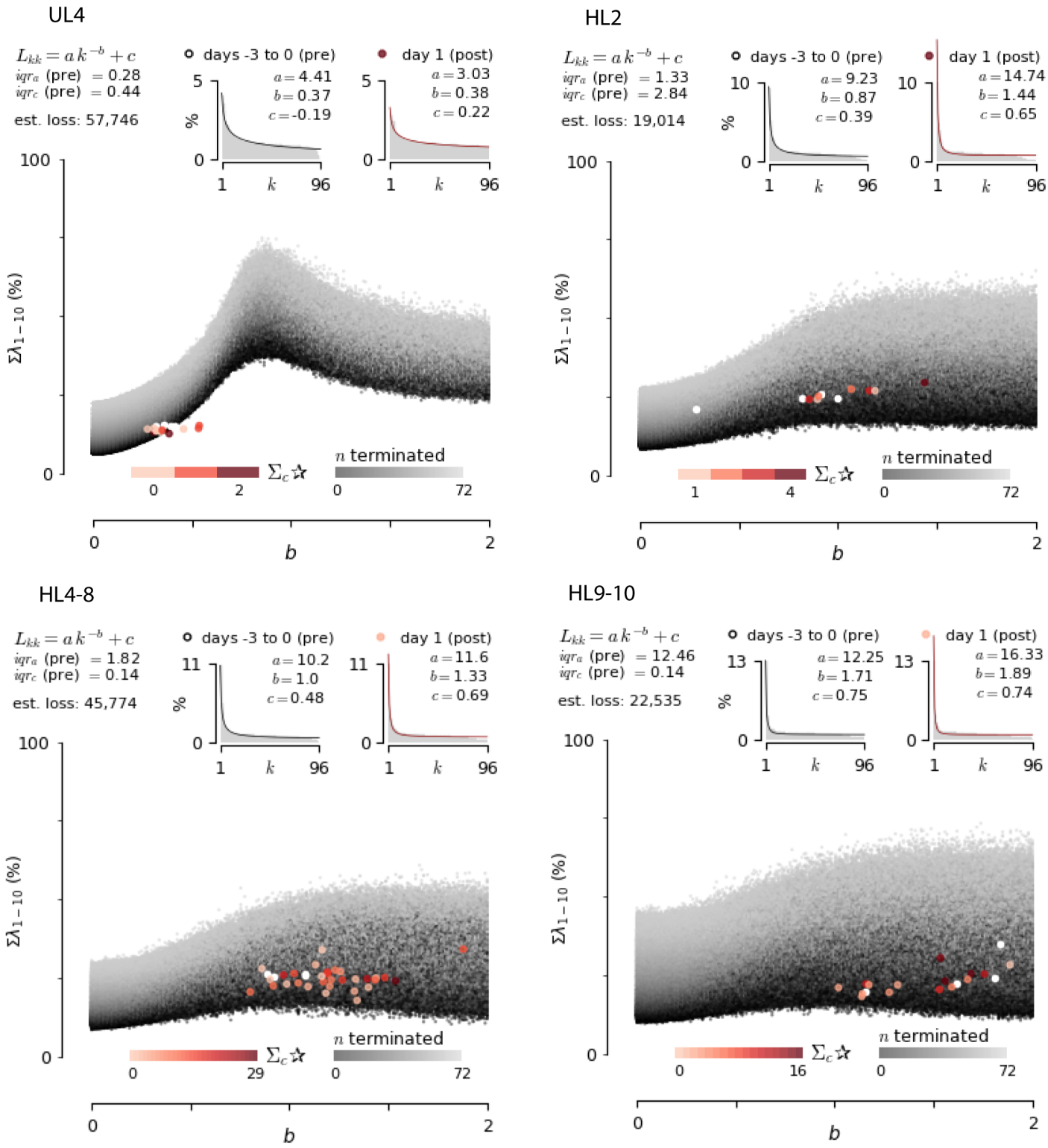

Figure S14:

The effect of neuron loss on the eigenvalues of sample covariance matrices. Spiking neural networks, each with 1000 neurons, were simulated in Nengo but only 96 neurons were sampled for analysis. Forty dimensions were now encoded, in an effort to promote stronger, more realistic contributions for the smaller eigenvalues ($geq10$). Although not perfect, an exponential function provided a sufficient fit to

the model's population covariance matrix eigenvalues. The median value for parameters a and c of the exponential model were determined by fitting 25 repeated model simulations with no neuron deletion (0.0 terminated; left inset). The scale parameter, b, was then swept to generate a range of different population eigenvalues, λ_{0-95} , $ae^{-bk}+c$, where $k \in [0,95]$ is the sorted eigenvalue number (largest to smallest). The simulated eigenvalues were used to create random covariance matrices from which n neurons could be terminated (described fully below). Next, the eigenvalues of these altered covariance matrices were determined and the top five were summed as a percentage of variance explained in the data. Only five eigenvalues were considered here instead of ten to avoid potential saturation at 100%. Plotting the results of the spiking neural network (red hues) over the numerical simulation (grey scale) demonstrates that lesion-evoked changes in population activity primarily affect the shape of the distribution, rather than a simple uniform increase, and that relative increases and decreases among the largest eigenvalues was a metric of interest that could easily be masked if simply summed (e.g., λ_2 might increase at the expense of λ_3). This suggested tracking the absolute value of the change in each of the largest eigenvalues normalized to their pre-lesion values. Combining the spiking neural network model with the numerical simulations provided a putative means to estimate neuron loss within a larger population using a small recorded sample. The right inset shows the predicted number of lost neurons in the entire network based on the recorded sub-sample and where it landed on the numerical simulation. Although a poor fit for the lower termination fractions, the model was able to tightly predict loss in the 0.4-0.9 range (both model and simulations experience substantial rank reduction in this regime). The imperfect fit to the eigenvalue distributions of the spiking neural network model is suspected to be responsible for poor estimation in the 0-0.35 range. For the in vivo data recorded from Monkey U and H, a power law $ak^{-b}+c$ fit the eigenvalue distributions well and has been used previously to describe distributions of eigenvalues in primate visual cortex.[163] The improved representation of the eigenvalue distributions apparently allowed for better estimation in the low termination range (0-0.3). The median of parameters a,c, and their inter-quartile ranges, $iqr_{a,c}$, were determined empirically for each animal and lesion across the associated pre-lesion days -3, -2, -1, and 0 (left panel inset). To simulate many noisy samples of the true population eigenvalue distribution, a uniformly random diagonal matrix drawn from $\mathcal{U}(iqr_c/2, iqr_c/2)$ was added to a diagonal matrix with entries λ_k, the eigenvalues of the generative model. This matrix was then multiplied by another uniformly random diagonal matrix, $\mathcal{U}(1-iqr_a/2, 1+iqr_a/2)$, in order to generate a noisy sample $\mathbf{S}$. The rationale was to mimic experimental conditions in which an electrode array records a small fraction of the local neuron population which has some hypothetical eigenspectrum specified by the best-fit parameters a,b,c. In order to generate a random covariance matrix with the specified eigenvalues, let $\mathbf{C}$ be a random, 96x96 real symmetric matrix, with eigen-decomposition given by $\mathbf{C} = \mathbf{QSQ}^{-1} = \mathbf{QSQ}^T$, where $\mathbf{Q}$ is an orthonormal matrix of 96 eigenvectors for $\mathbf{C}$. These random matrices $\mathbf{Q}$ were drawn from the $O(96)$ Haar distribution using the Scipy1.9.0 stats.ortho_group function and composed using $\mathbf{S}$ to obtain $\mathbf{C}$. Next, for each value of b and simulated array sample, "neurons" were terminated from the full population covariance matrices by setting $\mathbf{C}_{i,:} = \mathbf{C}_{:,i} = 0$ for n indices specified by uniform random draws from $[1,96]$. The termination number, n, is shaded in grey scale. After an in vivo lesion, the eigenspectrum shifts significantly for the ten largest eigenvalues. Like the spiking neural network model, these plots show that the scale parameter of the best fit varies significantly, while producing relatively little change in the sum of the top eigenvalues; this indicates that there are important increases and decreases in the variance explained by the largest eigenvalues beyond uniform shifts in the proportions of variance explained due to simple rank reduction that might occur with substantial population loss. Next, in vivo data from daily recording sessions were overlaid on the numerical simulations. The scale parameter b was determined as a best fit to the daily eigenspectrum determined for each lesion period, and the corresponding sum of the top ten eigenvalues. These values

are plotted as scatter points for each of the lesions performed in Monkeys U and H, with the color shaded according to the total daily behavioral deficit score. This allows estimation of neuron loss from the larger population, which we hypothesize to be reflected in the sample population's covariance. For the seven in vivo lesion groups from Monkey U and H, neuron loss was estimated for each by taking the largest post-lesion day's loss estimate and subtracting the median estimate for pre-lesion days. This fraction was then multiplied by the 267,000 neurons, described in the Discussion and Supplementary Figure S3, in order to generate an estimate number of terminated neurons.